Biogeosciences, 22, 305–321, 2025
https://doi.org/10.5194/bg-22-305-2025

Biogeosciences Open Access EGU

Research article

Ensemble estimates of global wetland methane emissions over 2000–2020

Zhen Zhang[1], Benjamin Poulter[2], Joe R. Melton[3], William J. Riley[4], George H. Allen[5], David J. Beerling[6], Philippe Bousquet[7], Josep G. Canadell[8], Etienne Fluet-Chouinard[9], Philippe Ciais[7], Nicola Gedney[10], Peter O. Hopcroft[11], Akihiko Ito[12], Robert B. Jackson[13], Atul K. Jain[14], Katherine Jensen[15], Fortunat Joos[16], Thomas Kleinen[17], Sara H. Knox[18,19], Tingting Li[20], Xin Li[1], Xiangyu Liu[21], Kyle McDonald[15], Gavin McNicol[22], Paul A. Miller[23], Jurek Müller[16], Prabir K. Patra[24,25], Changhui Peng[26], Shushi Peng[27], Zhangcai Qin[28], Ryan M. Riggs[29], Marielle Saunois[7], Qing Sun[16], Hanqin Tian[30], Xiaoming Xu[14], Yuanzhi Yao[31], Yi Xi[27], Wenxin Zhang[23,32], Qing Zhu[4], Qiuan Zhu[33], and Qianlai Zhuang[21]

[1]National Tibetan Plateau Data Center (TPDC), State Key Laboratory of Tibetan Plateau Earth System, Environment and Resource (TPESER), Institute of Tibetan Plateau Research, Chinese Academy of Sciences, Beijing, 100101, China
[2]NASA Goddard Space Flight Center, Earth Sciences Division, Greenbelt, MD, USA
[3]Climate Research Division, Environment and Climate Change Canada, Victoria, BC, Canada
[4]Climate and Ecosystem Sciences Division, Lawrence Berkeley National Laboratory, Berkeley, CA, USA
[5]Department of Geosciences, Virginia Polytechnic Institute and State University, Blacksburg, VA, USA
[6]Leverhulme Centre for Climate Change Mitigation, School of Biosciences, University of Sheffield, Sheffield, UK
[7]Laboratoire des Sciences du Climat et de l'Environnement, CEA, CNRS, UVSQ, Université Paris-Saclay, Gif-sur-Yvette, France
[8]Global Carbon Project, CSIRO Environment, ACT 2601, Australia
[9]Earth Systems Science Division, Pacific Northwest National Laboratory, Richland, WA 99352, USA
[10]Met Office Hadley Centre, Joint Centre for Hydrometeorological Research, Wallingford, UK
[11]School of Geography, Earth & Environmental Sciences, University of Birmingham, Birmingham, UK
[12]Graduate School of Agricultural and Life Sciences, the University of Tokyo, Tokyo, Japan
[13]Department of Earth System Science, Woods Institute for the Environment, and Precourt Institute for Energy, Stanford University, Stanford, CA 94305–2210, USA
[14]Department of Atmospheric Sciences, University of Illinois, Urbana, IL 61821, USA
[15]Department of Earth and Atmospheric Sciences, City College of New York, City University of New York, NY, USA
[16]Climate and Environmental Physics, Physics Institute and Oeschger Centre for Climate Change Research, University of Bern, Bern, Switzerland
[17]Department of Climate Dynamics, Max Planck Institute for Meteorology, Hamburg, Germany
[18]Department of Geography, University of British Columbia, Vancouver, BC, Canada
[19]Department of Geography, McGill University, Montreal, QC, Canada
[20]State Key Laboratory of Atmospheric Boundary Layer Physics and Atmospheric Chemistry (LAPC), Institute of Atmospheric Physics, Chinese Academy of Sciences, Beijing, 100029, China
[21]Department of Earth, Atmospheric, Planetary Sciences, Purdue University, West Lafayette, IN, USA
[22]Department of Atmospheric Sciences, University of Illinois, Chicago, IL, USA
[23]Department of Physical Geography and Ecosystem Science, Lund University, Sölvegatan 12, 223 62, Lund, Sweden
[24]Japan Agency for Marine-Earth Science and Technology (JAMSTEC), Yokohama, Japan
[25]Research Institute for Humanity and Nature (RIHN), Kyoto, Japan
[26]Department of Biology Sciences, University of Quebec in Montreal, C.P. 8888, Succ. Centre-Ville, Montreal, QC H3C 3P8, Canada
[27]Sino-French Institute for Earth System Science, Laboratory for Earth Surface Processes, College of Urban and Environmental Sciences, Peking University, Beijing, 100871, China

Published by Copernicus Publications on behalf of the European Geosciences Union.

[28]School of Atmospheric Sciences, Sun-Yat-Sen University, and Southern Marine Science and Engineering Guangdong Laboratory (Zhuhai), Zhuhai, 519000, China
[29]Department of Geography, Texas A&M University, College Station, TX, USA
[30]Center for Earth System Science and Global Sustainability, Schiller Institute for Integrated Science and Society, Department of Earth and Environmental Sciences, Boston College, Chestnut Hill, MA 02467, USA
[31]School of Geographic Sciences, East China Normal University, Shanghai, China
[32]School of Geographical and Earth Sciences, University of Glasgow, Glasgow, G12 8QQ, UK
[33]College of Hydrology and Water Resources, Hohai University, Nanjing, 210098, China

Correspondence: Zhen Zhang (yuisheng@gmail.com)

Received: 27 May 2024 – Discussion started: 11 June 2024
Revised: 26 October 2024 – Accepted: 8 November 2024 – Published: 15 January 2025

Abstract. Due to ongoing climate change, methane (CH_4) emissions from vegetated wetlands are projected to increase during the 21st century, challenging climate mitigation efforts aimed at limiting global warming. However, despite reports of rising emission trends, a comprehensive evaluation and attribution of recent changes remains limited. Here we assessed global wetland CH_4 emissions from 2000–2020 based on an ensemble of 16 process-based wetland models. Our results estimated global average wetland CH_4 emissions at 158 ± 24 (mean $\pm 1\sigma$) Tg CH_4 yr^{-1} over a total annual average wetland area of $8.0 \pm 2.0 \times 10^6$ km^2 for the period 2010–2020, with an average increase of 6–7 Tg CH_4 yr^{-1} in 2010–2019 compared to the average for 2000–2009. The increases in the four latitudinal bands of 90–30° S, 30° S–30° N, 30–60° N, and 60–90° N were 0.1–0.2, 3.6–3.7, 1.8–2.4, and 0.6–0.8 Tg CH_4 yr^{-1}, respectively, over the 2 decades. The modeled CH_4 sensitivities to temperature show reasonable consistency with eddy-covariance-based measurements from 34 sites. Rising temperature was the primary driver of the increase, while precipitation and rising atmospheric CO_2 concentrations played secondary roles with high levels of uncertainty. These modeled results suggest that climate change is driving increased wetland CH_4 emissions and that direct and sustained measurements are needed to monitor developments.

1 Introduction

Wetlands are the largest single source in the global methane (CH_4) budget, representing ~ 25–35 % of the total combined natural and anthropogenic sources (Kirschke et al., 2013; Saunois et al., 2016, 2020), with an uncertainty range of 100–230 Tg CH_4 yr^{-1} (Cao et al., 1996; Gedney et al., 2004; Bousquet et al., 2006; Petrescu et al., 2010; Spahni et al., 2011; Melton et al., 2013; Bridgham et al., 2013; Bloom et al., 2017; Poulter et al., 2017). Covering 8 %–10 % of the global land surface (Zhang et al., 2021a), wetland area is sensitive to climate variations (Zhang et al., 2018; Zhu et al., 2017). Over the last deglaciation, wetlands played an important role in driving the rise of atmospheric CH_4 concentrations (Hopcroft et al., 2017; Nisbet et al., 2023; Kleinen et al., 2023). In recent decades, wetlands have experienced unprecedented and ongoing changes, including continuous thawing of permafrost (Natali et al., 2019; Treat et al., 2018), land-use change (Fluet-Chouinard et al., 2023), a lengthening of the growing season in the Arctic (Arndt et al., 2019), and expansion in tropical areas due to enhanced precipitation (Fleischmann, 2023). Recent evidence from in situ measurements (Rößger et al., 2022), data-driven estimates (Yuan et al., 2024; Ying et al., 2024), and satellite observations (Feng et al., 2022) suggests that these ongoing changes could enhance wetland CH_4 emissions and thus affect the trajectory of the atmospheric CH_4 concentration. Furthermore, atmospheric δ^{13}C-CH_4 records also show a trend toward increased depletion since the late 2000s (Lan et al., 2021; Nisbet et al., 2019), indicating that isotopically light biogenic sources, such as wetlands (Basu et al., 2022; Feng et al., 2022), agriculture, and waste (Schaefer et al., 2016; Zhang et al., 2021b), have become dominant contributors to the rise in atmospheric CH_4. Current estimates of wetland CH_4 emissions (hereafter denoted as eCH_4) in response to climate change are projected to increase by up to 15 %–30 % by 2050 (Koffi et al., 2020; Zhang et al., 2017), accounting for 25 %–40 % of the pledged reduction in anthropogenic emissions (Shindell et al., 2019). These trends and projections suggest that the emerging wetland CH_4 climate feedback that influences atmospheric CH_4 concentration requires a better understanding of long-term changes in eCH_4.

Directly diagnosing the variations and trends of eCH_4 at large scales is challenging. Site-level measurements, such as those from chamber and eddy covariance techniques, are useful for identifying underlying mechanisms and monitoring CH_4 fluxes at the landscape scale but are difficult to upscale due to large uncertainties in extrapolation and the high spatial heterogeneity of wetland CH_4 fluxes (Chu et al., 2021; Kuhn et al., 2021). Interpreting eCH_4 using satellite observations

and inversions of atmospheric concentration data is also subject to uncertainties in anthropogenic sources, other natural sources, atmospheric chemistry, and model errors associated with atmospheric transport (Gatti et al., 2021; Gloor et al., 2021; Palmer et al., 2022; Patra et al., 2011; Zhang et al., 2021c). Global wetland models, integrated within land biosphere models, can serve to bridge our understanding of wetland CH_4 processes and diagnosing wetland CH_4 dynamics at large scales (Melton et al., 2013; Wania et al., 2013). These models provide mechanistic explanations for the causes of changes in eCH_4 dynamics. Furthermore, recent advances in wetland models (Arora et al., 2018; Kaiser et al., 2017; Shu et al., 2020; Grant, 2017; Chang et al., 2020) show significant potential for improving our understanding of eCH_4 through the incorporation of complex biogeochemical processes.

Current studies have reached various conclusions on the change in eCH_4 over the last decades. Studies based on single biogeochemical models (Zhang et al., 2018; Zhu et al., 2017) suggest a significant increase in eCH_4 from 2000–2006 to 2007–2017, while atmospheric inversions (Zhang et al., 2021c; Yin et al., 2021; Basu et al., 2022; Feng et al., 2022) suggested even higher rate increases from 2 to 3 Tg CH_4 yr^{-1} yr^{-1} during the post-2010 period. Poulter et al. (2017) reported no significant change between the 2000–2006 and 2007–2012 periods based on an ensemble of wetland models, while Saunois et al. (2020) show a slight increase (~ 2 Tg CH_4 yr^{-1}) on average for 2007–2017 compared to the 2000–2006 level using a large set of wetland CH_4 models. However, these models demonstrate considerable differences in estimated eCH_4, both spatially and temporally (Ma et al., 2021; Parker et al., 2020; Chang et al., 2023), primarily due to the sensitivity of their estimations to the wetland areal extent, the implemented biogeochemical structures, and parameterizations. The multi-model ensemble approach is applied to increase the skill, reliability, and consistency of model forecasts, potentially offsetting individual model errors (Schaefer et al., 2012). However, a recent study (Chang et al., 2023) found that downsampling atmospheric inversion and wetland model CH_4 predictions based on a comparison to eddy covariance data did not reduce uncertainty in global eCH_4 estimates. Therefore, it has become necessary to thoroughly evaluate the performance of these models using the most recent generation of wetland models against an increasingly dense network of observations (Delwiche et al., 2021; Knox et al., 2019) from eddy covariance sites.

Here we conducted ensemble simulations of 16 wetland biogeochemical models following a common modeling protocol to provide monthly integrated global eCH_4 for the period of 2000–2020, as part of the Global Carbon Project's methane budget activity. The inundation dynamics of each model were simulated using a model-specific prognostic hydrological modeling approach as well as a set of diagnostic satellite-driven simulations. A set of factorial simulations were carried out to isolate the effects of temperature, precipitation, and rising atmospheric CO_2 concentration. The modeled temperature sensitivity was evaluated against the global eddy covariance database FLUXNET-CH_4 (Delwiche et al., 2021; Knox et al., 2019) and a data-driven global wetland CH_4 upscaling dataset UpCH_4 (McNicol et al., 2023) based on FLUXNET-CH_4. In addition, we examined the changes in eCH_4 for the year 2020, which was characterized as an extremely warm and wet year with the highest growth rate of atmospheric CH_4 observed over the study period.

2 Methods

2.1 Wetland model ensemble

Sixteen wetland models participated in the ensemble simulations (Table S1). Wetland CH_4 models can be generally described as functions describing the biogeochemical processes that control CH_4 production and oxidation through methanogenesis and methanotrophy, as well as the biophysical processes that regulate CH_4 transport from the soil to the atmosphere (Table S1). Methanogenesis in the models is linked to different proxies (e.g., carbon substrate, heterotrophic respiration, net primary production) with a wide range of model complexity – more sophisticated models include wetland plant functional types (PFTs) and explicitly simulate the processes of CH_4 production, consumption, and transport, while the simplified models use generalized empirical equations to simulate net fluxes without explicitly calculating individual components of the CH_4 flux.

Wetlands were defined as naturally vegetated forested and non-forested ecosystems with saturated/inundated areas, excluding coastal wetlands; cultivated wetlands such as rice paddies; and open water systems such as rivers, lakes, ponds, and reservoirs. A prognostic wetland inundation scheme and a diagnostic wetland dataset (Wetland Area and Dynamics for Methane Modeling (WAD2M v2); Zhang et al., 2021a) were applied to identify the wetland areal dynamics. The prognostic wetland areal dynamics were independently determined by each model's hydrological modules, which use water table depth or soil moisture, combined with subgrid topographic conditions, to determine saturated areas within a land surface grid cell (Zhang et al., 2016; Xi et al., 2022). Among the participating models, there was a large variation in complexity and in the level of comprehensiveness with which wetland extents were characterized. The modules for simulating inundation ranged from simplified TOPMODEL approaches to more sophisticated representations of water table variation, with the estimated magnitude being influenced by the hydrologic schemes utilized and the sensitivities to precipitation. The prognostic modeled wetland extent showed large variability in estimated magnitude but was consistent with satellite-based inundation products in predicting different phases of inundation (Xi et al., 2022; Zhang, et al., 2021a). The ensemble mean of the modeled wetland extent

is close to 7.5×10^6 km^2 as estimated by WAD2M but higher than the 4.6×10^6 km^2 by the satellite-based product Global Surface Water Extent and Dynamics version 2 (GIEMS-2; Prigent et al., 2020). The modeled temporal variations in wetland areas show high correlations with satellite-based products for temperate regions and high latitudes (Fig. S1), except in the tropics. The limited agreement in the tropics may be due to the influence of aerosols and clouds on satellite-based measurements, as well as the process-based model's performance limitations in representing wetland areas. The diagnostic runs are exclusively used for temperature dependence calculations due to a discontinuity issue in WAD2Mv2 over a few tropical hotspots, which affect a subset of wetland models that are particularly sensitive to inundation in the hotspots.

2.2 Modeling protocol and simulation setups

The modeling protocol aimed to provide wetland CH_4 fluxes and quantify the associated uncertainties arising from model differences, meteorological forcing, and wetland extent dynamics. To quantify meteorological forcing uncertainty, we used two climate inputs: a ground-based monthly climate dataset from the Climatic Research Unit (CRU) (Harris et al., 2014) up to 2020 and a harmonized daily dataset from the Global Soil Wetness Project Phase 3 (GSWP3-W5E5) through the year 2019, which is a multiple-source-based daily dataset (Cucchi et al., 2020; Dirmeyer et al., 2006) used in the Inter-Sectoral Impact Model Intercomparison Project 3a (ISIMIP3a). For models that require 6-hourly meteorological forcings, a temporal-interpolation dataset (CRU-JRA) was applied based on the Japanese Reanalysis Agency (JRA55) aligned with CRU. The atmospheric CO_2 concentration values for 1861–2020 were obtained from the CMIP6 experimental protocol (Meinshausen et al., 2017). Ancillary data, such as soil texture and CH_4-related parameter sets, used model-specific inputs. All the models were run in "natural vegetation" mode without the transient effects of land-use or land-cover change. Methane oxidation in wetland soils was implicitly included in the estimate, but the upland oxidative sink was not included as it was not part of the net wetland emission calculations. Models included the spin-up period to pre-industrial conditions, assuming net ecosystem exchange equilibrium before 1860, by recycling fixed CO_2 concentrations (1860 level of 286.42 ppm) and meteorology (1901–1920).

2.3 FLUXNET-CH_4 and the machine learning-based upscaling product UpCH$_4$

FLUXNET-CH_4 is the first global dataset of CH_4 eddy covariance measurements that includes ~ 80 sites globally, including different wetland types such as peatlands (e.g., bog, fen), mineral wetlands (e.g., marsh, swamp), and rice paddies. For this study, a subset of natural freshwater wetland sites was selected for the analysis. All the eddy covariance measurements used in this study were gap-filled daily and total fluxes were filled using an artificial neural network (ANN) approach (Knox et al., 2019). In addition, a data-driven gridded dataset (UpCH$_4$; McNicol et al., 2023) for 2001–2018, which is based on 119 site-years of CH_4 fluxes from the FLUXNET-CH_4 dataset, was applied in the comparison. This dataset used a random forest model to upscale ground-based eddy covariance CH_4 flux data and was then forced with globally gridded predictor data and two wetland extent products to predict wetland CH_4 emissions. The predictors included data sources from climate, biometeorological, and soil properties.

2.4 Time series decomposition and statistical analyses

To attribute the time series of global wetland CH_4 emissions to what we consider the dominant drivers of change (i.e., temperature, precipitation, and CO_2 concentration), we applied a multiple regression approach (Piao et al., 2013) to estimate the parameters of global wetland CH_4 sensitivity to climate drivers using the following equation:

$$y = \beta \mathrm{CO_2} + \gamma \mathrm{Tmp} + \delta \mathrm{Pre} + c + \varepsilon, \quad (1)$$

where y is the global annual total wetland CH_4 emission of each model from the transient run or from the observation-based upscaling dataset UpCH$_4$, and Tmp, Pre, and CO_2 are the mean annual temperature, total annual precipitation, and mean atmospheric CO_2 concentration for that year, respectively. γ, δ, β, and c are regression coefficients, and ε is the residual error term. The regression coefficients were calculated using a maximum likelihood estimate. Changes in other meteorological forcings may also influence the estimation of y. These confounding drivers, such as solar radiation and wind speed, although they are considered to have minor impacts on the variations of eCH$_4$, were implicitly accounted for in the regression coefficients.

2.5 Model factorial experiment

To further separate the contribution of different controls on the change in methane emissions (ΔeCH$_4$) by climate variations and rising CO_2, we used a subset of four models that conducted factorial experimental simulations by holding each factor constant during part of the transient runs. This subset of the wetland models (i.e., four wetland models: ELM-ECA, LPJ-wsl, SDGVM, and VISIT) performed a set of factorial simulations to specifically attribute the effect of temperature, precipitation, and rising CO_2 concentration on wetland CH_4 fluxes with the climatology of 2000–2006 for 2007–2020. The simulations were performed by running the model while keeping one factor constant at a time to estimate the contribution of each component to the total range of variations (Table S2). For these factorial simulations, we evaluated the annual amplitude of wetland eCH$_4$ as a relative

percentage change to minimize the impacts of different modeling implementation choices, such as different input variables among models. The effect of the total changes on the relative change in amplitude was represented by the difference between the transient (one factor is time-varying) and baseline (static at 2000–2006 levels) runs. For simplicity, the relative contribution of a single driver to eCH_4 variations was quantified as the transient run minus the specific control run. To calculate the contribution of each driver using the subset of the models, we calculated weighting factors per year across the models, with lower bias resulting in higher weight relative to the full ensemble mean using an inverse function.

2.6 Temperature dependence calculation

To further evaluate the response of eCH_4 to rising temperatures, we calculated the modeled seasonal eCH_4 temperature dependence, referred to as the apparent Q_{10} metric at the locations of 34 FLUXNET-CH_4 sites. This seasonal Q_{10} differs from the intrinsic Q_{10} prescribed in the parameterization of respiratory processes in each model. Here it represents the overall response of eCH_4 along geographic temperature gradients. The apparent Q_{10} is defined as eCH_4 sensitivity to temperature change. We calculated apparent Q_{10} based on CH_4 emitting strength over a standard wetland area, which was calculated as the CH_4 fluxes divided by inundated area on a per-pixel basis to exclude the effect of inundation dynamics. To derive the temperature dependence of eCH_4 at the soil or ecosystem level, we applied the following equation:

$$R(i) = R_{\mathrm{b}}(i) Q_{10}^{\frac{T(i) - T_{\mathrm{ref}}}{\Gamma}}, \quad (2)$$

where $R(i)$ is the net wetland flux at the location of site i, $R_{\mathrm{b}}(i)$ is the basal net CH_4 flux at the reference temperature T_{ref}, and $T(i)$ is ambient temperature. The parameters Q_{10}, $\Gamma = 10°$, and $T_{\mathrm{ref}} = 15°$ are all time-independent constants. The Q_{10} acting on specific timescales can be obtained from eCH_4 at corresponding specific timescales (i.e., seasonal total and annual total) by fitting an exponential regression with modeled eCH_4 and air temperature from CRU or GSWP3-W5E5. To quantify the uncertainty in observed apparent Q_{10}, we employed 1000 sets of resampled FLUXNET-CH_4 observations generated based on a Gaussian distribution. The uncertainty range in measured seasonal mean CH_4 fluxes was determined by aggregating the uncertainty of daily total fluxes obtained through ANN gap filling.

3 Results and discussion

3.1 Changes in eCH_4 during the period 2000–2020

The multi-model ensemble based on the prognostic inundation schemes shows that the average annual global eCH_4 over the period 2000–2020 was 156 ± 24 Tg CH_4 yr^{-1} (mean $\pm 1\sigma$). The average annual eCH_4 increased from 153 ± 23 Tg CH_4 yr^{-1} during 2000–2009 to 158 ± 24 Tg CH_4 yr^{-1} during 2010–2020. And 15 out of 22 model simulations show significant positive linear trends ($p<0.01$), with an ensemble mean increase rate of 0.6 ± 0.3 Tg CH_4 yr^{-1} yr^{-1} over 2000–2020 (Fig. 1a; Table 1; Fig. S2). Differences in total annual emissions between the two sets of simulations driven by two different climate datasets (CRU and GSWP3-W5E5) agree well in the magnitude of the annual anomalies. Notable eCH_4 variations to climate events were observed, such as the rise during the 2010 La Niña (+5.2 Tg CH_4 yr^{-1}) and the decline during the 2015 El Niño (-4.6 Tg CH_4 yr^{-1}) after removing the positive linear trends. The multi-model ensemble wetland eCH_4 response to climate events is consistent with those reported by earlier studies (Zhang et al., 2018; Zhu et al., 2017) using single wetland models, indicating a modulation of the phase of eCH_4 anomaly (ΔeCH_4) by the El Niño–Southern Oscillation. The model ensemble demonstrates a consistent increase in interannual variability (IAV) in ΔeCH_4 from 3.6 ± 1.6 Tg CH_4 yr^{-1} during 2000–2009 to 4.7 ± 1.5 Tg CH_4 yr^{-1} during 2010–2020, suggesting a potential increase in eCH_4 variability under climate change.

The models consistently show that 2020 is the strongest positive anomaly year during 2000–2020, with a net increase of 2 [−2, 7] Tg CH_4 yr^{-1} (mean [min, max]) in 2020 compared to 2019. This positive anomaly in 2020 (Table 1) is broadly consistent with a recent study (Peng et al., 2022) that reported 6 ± 2.3 Tg CH_4 yr^{-1} based on simulations of two bottom-up models with different climate datasets. The discrepancy in estimated magnitude between the Peng et al. (2022) and our results is partly due to the parameterizations of the CH_4 module that causes lower annual magnitude in this study ($\sim 162 \pm 23$ Tg CH_4 yr^{-1} in 2020) compared to the Peng et al. (2022) study (177 ± 31 Tg CH_4 yr^{-1} in 2020). Additionally, the precipitation inputs in the climate forcing used in this study show a lower positive anomaly ($\sim$ of 20 mm yr^{-1} in CRU over global wetland) in precipitation in 2020 compared to the reanalysis-based estimates ($\sim$ 40–117 mm yr^{-1}) over global wetlands used in the study by Peng et al. (2022), which leads to lower estimates of wetland area and consequently lower emissions in this study. Moreover, our model ensemble does not indicate a strong increase (-0.2 [−1.5–0.7] Tg CH_4 yr^{-1}) in eCH_4 in Africa in 2020. This contrasts with recent atmospheric inversions (Feng et al., 2023; Qu et al., 2022), which suggest a large increase of 11–17 Tg CH_4 yr^{-1} above 2019 levels in African CH_4 emissions for 2020. The estimated increase from these inversions is equivalent to 55 %–85 % of total eCH_4 in Africa during 2010–2019 in our study (Fig. 2). These discrepancies highlight the need for further studies to investigate the differences between these two approaches, including uncertainty in climate inputs in process-based bottom-up models and partitioning different sources in atmospheric inversions.

There were widespread net increases in eCH_4 across all latitudinal bands during 2010–2020, compared to the av-

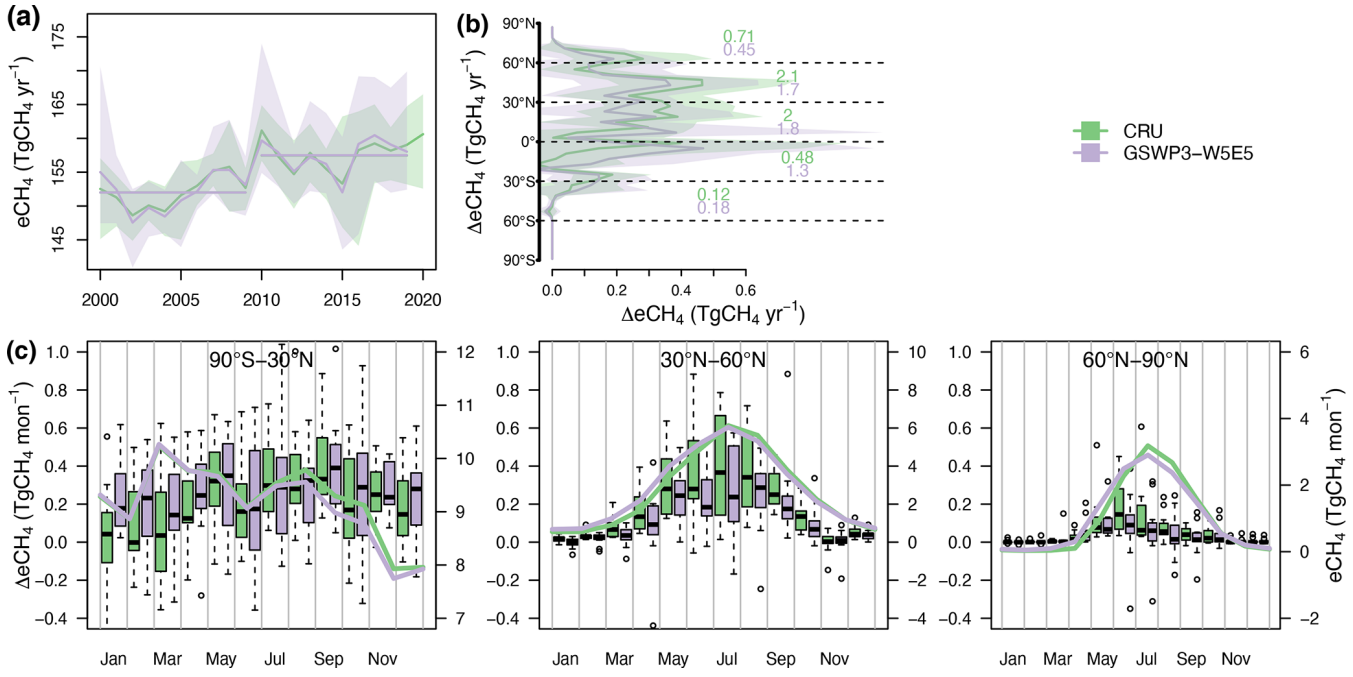

Figure 1. Simulated global wetland CH_4 emissions from the model ensemble for 2000–2020. **(a)** Time series of annual total emissions during 2000–2020, with the shaded area representing the range between minimum and maximum modeled emissions. The horizontal lines represent the ensemble means of 2000–2009 (152 Tg CH_4 yr^{-1}) and 2010–2019 (158 Tg CH_4 yr^{-1}), respectively. **(b)** Latitudinal gradient of eCH_4 difference (ΔeCH_4), with the mean annual total ΔeCH_4 for each of the 30° latitude bins from the two sets of simulations shown. The change is calculated relative to the mean of the 2000–2009 level from the two sets of simulations with prognostic wetland emission models grouped by different climate datasets, CRU and GSWP3-W5E5. **(c)** Boxplots of mean seasonal ΔeCH_4 for the three regions. The central mark and the bottom and top edges of the box indicate the median and the 25th and 75th percentiles of the ensemble, respectively. The colored lines represent the average seasonal cycle of 2000–2009 from the simulations grouped by two climate datasets, CRU and GSWP3-W5E5.

erage of 2000–2009, with the largest magnitudes occurring in the 90° S–30° N bands (there are relatively few wetlands in the southern extratropics of 90–30° S, contributing 0.1–0.2 Tg CH_4 yr^{-1}) and temperate regions (30–60° N) (Fig. 1b). The annual magnitude of eCH_4 increased by 3.7–3.8, 1.8–2.4, and 0.6–0.8 Tg CH_4 yr^{-1} in the tropical, temperate, and Arctic wetlands, respectively. The tropics have experienced the largest increases in annual total emissions with an increase of 3 % relative to 2000–2009 (Table 1). This finding is aligned with the results of several recent atmospheric inversions (Basu et al., 2022; Feng et al., 2022; Lan et al., 2021) using satellite observations and/or isotopic measurements that suggest a large increase in microbial emissions for the post-2007 period in the tropics. While the increase in annual total emissions from temperate wetlands is lower than that from the tropics, they nevertheless show a larger relative increase of 5 %–8 % compared to 2000–2009. Arctic wetlands also show an increased rate of 5 %–7 % relative to the same period.

The increase in eCH_4 occurs in parallel with differing patterns of enhanced seasonal cycles between tropical and extratropical wetlands (30–90° N) (Fig. 1c). In temperate and Arctic wetlands, the majority of the increase in emissions (60 %–92 %) occurred primarily during the growing season (May–October). Specifically, increases in Arctic wetlands occurred during the early growing season (May–July), aligning with findings from a data-driven estimate (Yuan et al., 2024) and a long-term eddy-covariance-based study (Rößger et al., 2022) that observed early-growing-season increases in eCH_4 due to continuous warming in a Siberian wetland. In contrast, the increase in emissions within the 90° S–30° N band exhibited relatively minor seasonal variations throughout the year, with the May–October period accounting for a 24 % greater increase in ΔeCH_4 compared to the November–April period (Fig. S3).

3.2 Spatial distribution of eCH_4

A few key regions contribute significantly to global emissions (Fig. 2a, c). These regions are mainly floodplains located along major river basins such as the Amazon, Ganges, Mississippi, and Yangtze; tropical peatlands in the Congo and Southeastern Asia; and high-latitude peatlands in the Hudson Bay Lowland (HBL) and West Siberian Lowland (WSL). However, inter-model variabilities in eCH_4 reveal varying levels of spatial agreement between models, with the largest discrepancies coming from South America and Africa. South America is one of the largest contributors to the

Table 1. Summary of wetland CH_4 emissions (Tg CH_4 yr^{-1}) over different time periods by latitudinal bands for the prognostic wetland simulations. The ensemble mean with minimum and maximum (numbers within square brackets) are listed, respectively.

Time period	Forcing	90–30° S	30° S–30° N	30–60° N	60–90° N	Global
2000–2009	CRU	3[1–5]	107[63–141]	31[16–60]	11[4–29]	152[119–187]
	GSWP3-W5E5	3[1–5]	106[60–142]	33[18–57]	11[4–29]	153[116–188]
2010–2019	CRU	3[1–6]	110[67–144]	34[17–64]	12[4–30]	158[126–193]
	GSWP3-W5E5	3[1–6]	110[64–146]	35[18–60]	12[4–29]	158[118–203]

global total eCH_4. Still, the net change in that region shows only a moderate increase, with diverging trends within the Amazon Basin during the 2010s (Fig. 2b, d). The uncertain temporal trends are consistent with a long-term, large-scale atmospheric inversion based on airborne campaigns (Basso et al., 2021). South Asia and Africa are among the regions with the largest increases in the tropics, next to North America, but have high uncertainty with a lower level of agreement among the models (Fig. S4). The model ensemble shows that northwestern South Asia has a significant percentage increase in eCH_4 during 2010–2019 relative to its average levels from 2000–2009, suggesting a possible high sensitivity of eCH_4 to climate change in this region.

The comparison with previous estimates from bottom-up approaches and top-down atmospheric inversions (Table S3) suggests that the model ensemble mean generally captures well the spatial distribution of annual eCH_4, with a potential underestimation for a few methane hotspots (Fig. S5). The model ensemble means for the Amazon Basin, HBL, and WSL show good agreement with atmospheric inversions (Bergamaschi et al., 2013; Pickett-Heaps et al., 2011; Ringeval et al., 2014; Tunnicliffe et al., 2020; Wilson et al., 2016, 2021) and bottom-up modeling estimates (Bansal et al., 2023; Bloom et al., 2017; Bohn et al., 2015), with relatively low uncertainty. The model ensemble highlights WSL and HBL as CH_4 hotspots in the high latitudes, with good agreements of annual magnitudes with atmospheric inversions and in situ observations (Bohn et al., 2015; Glagolev et al., 2011; Pickett-Heaps et al., 2011), while the models have lower estimates for Alaska compared to the inversions (Chang et al., 2014; Miller et al., 2016). However, for the two hotspots of the Pantanal and Sudd wetlands, the models tended to underestimate the annual eCH_4 compared to a few recent satellite-based estimates (Gerlein-Safdi et al., 2021; Gloor et al., 2021; Lunt et al., 2021; Pandey et al., 2021), with a large uncertainty range of up to 2 orders of magnitude across the model ensemble (Fig. S5). In addition to the regions where eCH_4 are being underestimated, recent studies (France et al., 2022; Shaw et al., 2022) based on aircraft measurements suggest that the bottom-up models likely underestimate high eCH_4 fluxes in some little-studied wetlands, such as those in Zambia and Bolivia. The underestimations by process-based wetland models can be attributed to (1) the challenge in accurately capturing the areal dynamics of wetlands under varying hydrological conditions, such as in flat terrains that receive lateral transport of water from upper streams (Li et al., 2024; Lunt et al., 2021; Gerlein-Safdi et al., 2021); (2) existing knowledge gaps in mapping wetlands in remote areas, which affect the parameterization of inundation modeling; and (3) the limited representation of water table regulation (Chen et al., 2021) and wetland PFTs (Bastviken et al., 2023) on eCH_4 in biogeochemical models.

3.3 Attribution of wetland CH_4 changes

To evaluate the relative contribution of different factors on global eCH_4, we calculated the sensitivity of eCH_4 to mean annual temperature (denoted as γ), annual total precipitation (denoted as δ), and CO_2 concentration (denoted as β) using a multiple regression approach for each model run over the period of 2000–2020. The same approach was applied to the upscaled gridded machine learning dataset $UpCH_4$, which uses eddy covariance measurements from FLUXNET-CH_4 as training inputs. The model ensemble suggests that temperature is the primary driver of the increase in eCH_4 (Fig. 3a). The regression coefficient for γ is 4.6 Tg CH_4 yr^{-1} $°C^{-1}$, with a range of -0.4 and 9.0 Tg CH_4 yr^{-1} $°C^{-1}$ between the 10th and 90th percentiles among all models. This mean temperature sensitivity is slightly higher than the γ coefficient of 3.2–4.1 Tg CH_4 yr^{-1} $°C^{-1}$ estimated for $UpCH_4$. In contrast, precipitation contributed little to the increase from the prognostic simulations, with a coefficient δ of 0–0.3 Tg CH_4 yr^{-1} mm^{-1}. The coefficient δ was lower at -0.05–0 Tg CH_4 yr^{-1} mm^{-1} for $UpCH_4$, as precipitation was not chosen as a model training predictor through its feature selection, based on site-level eddy covariance measurements (McNicol et al., 2023). However, precipitation is a more dominant factor at large scales, especially for tropical floodplains, which contribute the largest proportion of emissions but are poorly represented by eddy covariance measurements. The model-ensemble-estimated β remains small, ranging from 0 to 0.3 Tg CH_4 yr^{-1} ppm^{-1}, while $UpCH_4$ suggests a β at -0.01 Tg CH_4 yr^{-1} ppm^{-1}. However, other confounding drivers might influence eCH_4 as well, such as solar radiation, wind speed, and nitrogen deposition. Thus, the inferred sensitivities are implicitly accounted for in the regression coefficients despite their relatively small impacts compared to the major drivers.

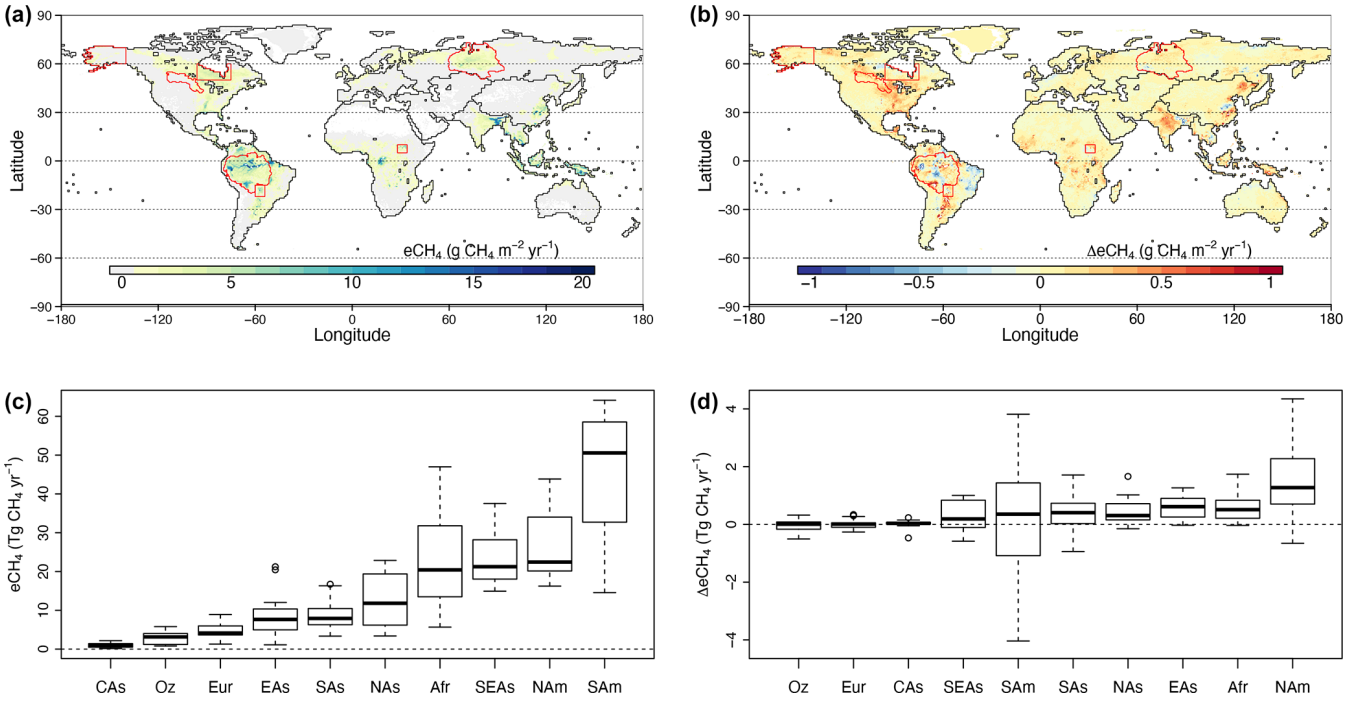

Figure 2. Spatial distribution of eCH_4 and the average change between the 2010s and 2000s. **(a)** Map of mean eCH_4 (unit: g CH_4 m^{-2} yr^{-1} per 0.5° grid cell) for 2000–2020. The regions defined in panels **(c)** and **(d)** and regional CH_4 hotspots in Table S3 are outlined in black and red, respectively. **(b)** Map of change in mean annual wetland emissions (ΔeCH_4) between the 2010s and 2000s. **(c)** Boxplot of mean annual eCH_4 and **(d)** ΔeCH_4 by regions for 2000–2020 in ascending order for median estimates. Afr: Africa; CAs: Central Asia; EAs: East Asia; Eur: Europe; NAm: North America; NAs: North Asia; Oz: Oceania; SAm: South America; SAs: South Asia; SEAs: Southeast Asia.

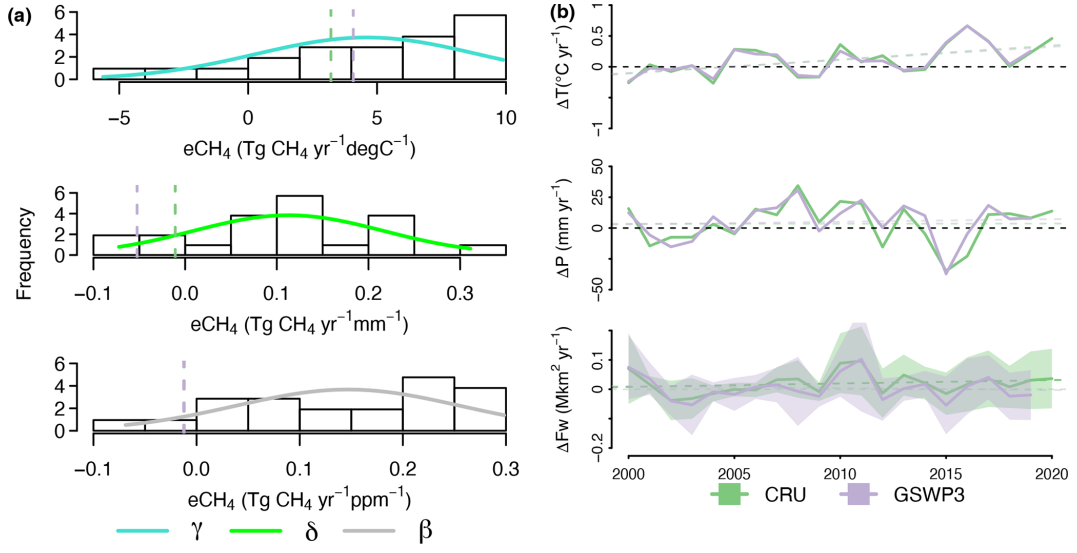

Figure 3. Attributions of ΔeCH_4 during 2000–2020. **(a)** Histogram showing the sensitivity coefficients derived from a multiple regression approach (see the Methods section) for temperature (γ), precipitation (δ), and atmospheric CO_2 concentration (β). The curves represent probability distributions of sensitivity coefficients across the models, assuming a Gaussian distribution. Vertical lines represent estimates from the machine learning-based dataset $UpCH_4$, with different colors corresponding to different climate datasets. **(b)** Time series of anomalies for annual mean temperature (ΔT), annual total precipitation (ΔP), and annual mean wetland extent (ΔFw) for 2000–2020 for CRU and 2000–2019 for GSWP3. The shaded areas in ΔFw represent the minimum and maximum ranges from the prognostic model simulations. Dashed lines are linear fitted trends for the corresponding variables.

Generally, the factorial simulations of the four-model subset indicated a consistently positive contribution (three out of four) from rising temperature to ΔeCH_4, with a large variability (SD = 4.3 Tg CH_4 yr^{-1}) of contributions from precipitation (Fig. S6). The strength of the CO_2 fertilization effect varied among models and was moderate but positive in all models. Two models (ELM-ECA and SDGVM) were among the models with higher sensitivity to climate variations, while LPJ-wsl and VISIT were close to the full ensemble mean. ELM-ECA produced a negative temperature effect on eCH_4, likely due to its modeled nutrient constraints and higher temperature sensitivity for methanotrophic compared to methanogenic processes. Considering the deviation of each model from the full ensemble mean, the weighted mean (Fig. S7) contributions for temperature, precipitation, and CO_2 concentration from the subset models were 3.2, 1.8, and 1.4 Tg CH_4 yr^{-1}, respectively. The results from the subset of the models consistently demonstrate that temperature is the primary factor influencing eCH_4.

Overall, the interannual variations of modeled eCH_4 were primarily associated with rising temperature, altered precipitation patterns, and rising atmospheric CO_2 concentrations that stimulated ecosystem productivity through the CO_2 fertilization effect (Yvon-Durocher et al., 2014). We note that a recent study found strong hysteresis in the seasonal temperature dependence of observed eCH_4 using the FLUXNET-CH_4 dataset (Chang et al., 2021). Those hysteretic features likely result in uncertainty in annual temperature sensitivity estimates but would not bias the conclusion of temperature as a dominant controller of eCH_4 at the decadal timescale. The links between rising temperature and enhanced net CH_4 fluxes are evident (as described below), as the annual global average temperature over wetland areas has significantly (p<0.01) increased by 0.5–0.7 °C from 2000–2020 (Fig. 3b). The modeled interannual variations of wetland extent dynamics reproduced the response to strong climate events (e.g., positive anomaly during the La Niña phase in 2010/2011 (Boening et al., 2012) and 2020). Both climate-forcing datasets suggest no significant trend in the anomaly of annual mean wetland area globally over the same period based on the prognostic hydrological simulations (Fig. 3b). Similarly, no significant regional trends in wetland area were found for most of the subregions, with the exception of South America, which shows a decrease, and East Asia, which shows a slight increase (Fig. S8). Considering that the extent of modeled wetland areas is primarily driven by precipitation, we do not detect a substantial contribution of changes in wetland extent to the long-term increase in eCH_4 over 2000–2020 based on the climate datasets. However, considerable differences in annual and seasonal precipitation estimates between the climate datasets used in this study and those derived from reanalysis or satellite-based products (Zhang et al., 2023a) result in large uncertainties in the estimated trends in wetland extent.

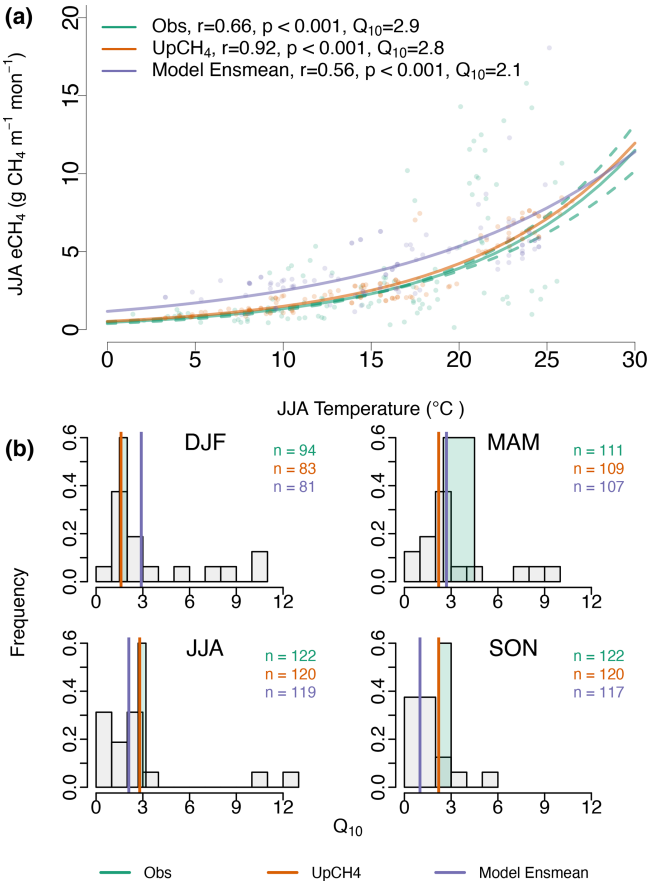

Figure 4. Temperature dependence of simulated seasonal eCH_4 across locations of FLUXNET-CH_4 sites. **(a)** Model ensemble mean ("Model Ensmean") of simulated eCH_4 against seasonal mean temperature for the JJA season along the temperature gradient at the locations of FLUXNET-CH_4 sites in comparison to the estimates from eddy covariance measurements ("Obs"; Fig. S10; Table S4) and $UpCH_4$. Each dot represents the value at one site for an individual year when observations are available. The unit of the simulated CH_4 emissions is gCH_4 m^{-1} $month^{-1}$ per standard wetland area to exclude the effect of inundation on eCH_4. The exponential fitted curves are shown. **(b)** Histogram of the seasonal Q_{10} for the 16 individual models for the months of DJF, MAM, JJA, and SON. Sample sizes are shown in the plot. The Q_{10} values derived from FLUXNET-CH_4, $UpCH_4$, and the model ensemble mean are shown as vertical solid lines, with a width of the bar for "Obs" indicating the uncertainty range of Q_{10} based on measurement uncertainty.

3.4 Temperature dependence of wetland CH_4 models

The modeled CH_4 emissions show an exponential relationship between eCH_4 and air temperature, with higher temperatures corresponding to higher mean eCH_4 during the peak growing season (JJA, June–July–August) in the Northern Hemisphere (Fig. 4a). The model ensemble mean of eCH_4 response to temperature shows good agreement within the range of the spread when compared to the site-level measurements from FLUXNET-CH_4 and the gridded product

$UpCH_4$. The model ensemble mean has a higher CH_4 emitting strength (i.e., CH_4 emission per standard wetland area) for the high latitudes, leading to lower apparent Q_{10}. This implies that the model-ensemble-estimated temperature dependence for the high latitudes could be potentially overestimated during the JJA season. The apparent Q_{10} values for individual models show a large spread (Fig. S9), with 11 out of the 16 models having statistically significant ($p<0.01$) exponential relationships. The good agreement between the ensemble mean and observations suggests that the ensemble approach provides a better constraint compared to single models alone. Furthermore, it is important to acknowledge that the sparse spatial coverage of FLUXNET-CH_4 over low latitudes, especially for underrepresented areas such as Africa, Southeast Asia, and South America, limits our ability to evaluate temperature dependencies over high-temperature regions (Fig. S10).

The modeled apparent Q_{10} exhibits an average temperature dependence similar to that of ecosystem respiration, as reported by previous studies (Bloom et al., 2017; Mahecha et al., 2010; Yvon-Durocher et al., 2014), indicating that the underlying factors controlling the response of eCH_4 and ecosystem respiration to temperature covary. The modeled temperature dependences are more constrained with less spread for JJA and SON (September–October–November) than DJF (December–January–February) and MAM (March–April–May) when most site-level measurements have limited availability. The seasonal variations of modeled apparent Q_{10} differ from site-level observations or $UpCH_4$, reflecting discrepancies in the involved processes between eddy covariance and land surface models. Given that underrepresented processes such as substrate supply tend to have higher sensitivity of ecosystem metabolic processes to temperature, it is likely that the models do not entirely capture the fine-scale processes that affect the overall temperature response (Chang et al., 2021). In addition, the absence or underrepresentation of certain biophysical processes could lead to lower modeled apparent Q_{10}. For instance, the ensemble mean of modeled apparent Q_{10} for SON months is underestimated, likely linked to the limited representation of processes during the freeze–thaw cycle (e.g., zero-curtain period), as suggested by previous observational studies (Mastepanov et al., 2008; Zona et al., 2016).

4 Conclusions

Our results estimated global average wetland CH_4 emissions at 158 ± 24 (mean $\pm 1\sigma$) Tg CH_4 yr^{-1} for the period 2010–2020, with an average decadal increase of 6–7 Tg CH_4 yr^{-1} compared to the decade of 2000–2009. The increases in the four latitudinal bands of 90–30° S, 30° S–30° N, 30–60° N, and 60–90° N were 0.1–0.2, 3.6–3.7, 1.8–2.4, and 0.6–0.8 Tg CH_4 yr^{-1}, respectively, during the 2 decades. Our analysis reveals how global wetlands respond to variations in the primary climatic controls of temperature, precipitation, and rising CO_2 concentrations. The model average shows good agreement with eddy covariance measurements on temperature dependence, confirming the primary role of temperature in the rising trajectory of eCH_4 at decadal timescales. Furthermore, the modeled ensembles of prognostic wetland extents offer a complementary approach to satellite-based estimates (Prigent et al., 2020; Zhang, et al., 2021a) and enable further investigation into the uncertainties in wetland area estimation. These differences can motivate improvements to inundation schemes through an improved water table position (Chen et al., 2021) and lateral flow representation. Note that a large portion of tropical wetlands comprise inundated floodplains connecting rivers, where the leaching of methane production from wetlands to river networks is not accounted for in the wetland models. The prognostic models estimate an annual mean maximum wetland area of $8.0 \pm 2.0 \times 10^6$ km^2, with a seasonal cycle (annual maximum minus annual minimum) of $4.7 \pm 2.0 \times 10^6$ km^2. Resolving the large uncertainty in wetland areas and seasonal variation remains a high priority to refine bottom-up estimates of eCH_4. Lastly, our results highlight the important but highly uncertain CO_2 fertilization effect on eCH_4. The mean sensitivity coefficient β and results from the factorial experiment suggest a net increase in eCH_4 of 0.1 %–2.3 % relative to the annual total under an average ~ 20 ppm increase in atmospheric CO_2 concentration. In comparison, a synthesis study based on field experiments (van Groenigen et al., 2011) shows a narrower range of 0.3 %–0.6 % average increase for every 20 ppm increase, assuming a linear fertilization effect between CO_2 concentration and eCH_4.

Our results show that an ensemble of process-based wetland methane models provides quantification for uncertainty in eCH_4, as well as better constraints than a single model on the predicted trend and magnitude of eCH_4. However, nominally distinct models might have similar biases because of similarities in the way they represent a subset of processes (see Table S1 for the model summary). Future evaluation of modeled processes, such as oxidation, production, and transport pathways, along with model errors across different timescales using statistical tools, could help identify similarities in model behaviors to guide model development (Zhang, 2023b). Furthermore, the eCH_4 estimates are subject to forcing uncertainty, given that the two climate datasets applied in the simulation protocol do not cover the full magnitude and variability of climatic variables. Specifically, precipitation has a significant impact on wetland extent and anaerobic soil conditions but has large uncertainty in spatiotemporal patterns (Sun et al., 2018). Thus, we recommend that future ensemble simulations consider the uncertainty in climate variables among different datasets. In addition, the sensitivity parameters derived from the multiple regression are not independent of climate datasets. Thus, they are affected by the choice of meteorological drivers. Overall, quantitatively accounting for model performance and dependence

and thoroughly evaluating the effectiveness (Chang et al., 2023) could improve the wetland model ensemble estimation in future studies.

Code and data availability. The code for the wetland models is available upon request from the respective model groups. The wetland ensemble results are publicly available in the Zenodo repository at https://doi.org/10.5281/zenodo.11309188 (Zhang, 2024). The wetland estimates from individual models are available upon request from the respective model groups. The FLUXNET-CH_4 dataset is publicly available at the following link: https://fluxnet.org/data/fluxnet-ch4-community-product/ (last access: 28 December 2024, FLUXNET-CH4 Community Product, 2024). The UpCH_4 dataset can be found at the link in McNicol et al. (2023).

Supplement. The supplement related to this article is available online at: https://doi.org/10.5194/bg-22-305-2025-supplement.

Author contributions. BP and ZZ designed the simulation experiment with contributions from JM and WR. ZZ conducted data collection and data analysis. JM, WR, GB, PC, NG, PH, AI, AJ, FJ, TK, TL, XL, PM, JM, CP, SP, ZQ, QS, HT, XX, YY, XY, WZ, QinZ, QiuZ, QiaZ, and ZZ performed the simulations. ZZ prepared the manuscript with contributions from all co-authors.

Competing interests. At least one of the (co-)authors is a member of the editorial board of *Biogeosciences*. The peer-review process was guided by an independent editor, and the authors also have no other competing interests to declare.

Disclaimer. Publisher's note: Copernicus Publications remains neutral with regard to jurisdictional claims made in the text, published maps, institutional affiliations, or any other geographical representation in this paper. While Copernicus Publications makes every effort to include appropriate place names, the final responsibility lies with the authors.

Acknowledgements. This paper is the result of a collaborative international effort under the umbrella of the Global Carbon Project, a project of Future Earth, and a research partner of the World Climate Research Programme. Joe R. Melton thanks Jade Skye for her assistance in running and processing the CLASSIC model simulations.

Financial support. Zhen Zhang acknowledges support from the National Natural Science Foundation of China Basic Science Center for Tibetan Plateau Earth System project. Yi Xi and Shushi Peng were funded by NSFC (41830643, 41722101). Thomas Kleinen acknowledges support from the German Federal Ministry of Education and Research ((BMBF) grant no. 01LP1921A). Akihiko Ito and Prabir Patra were partly supported by the Arctic Challenge for Sustainability II (ArCS-II) project (grant no. JPMXD1420318865), funded by Japan's Ministry of Education, Culture, Sports, Science and Technology (MEXT). Xiangyu Liu and Qianlai Zhuang are supported by a NASA project (NNX17AK20G). Qiuan Zhu and Changhui Peng are supported by the Second Tibetan Plateau Scientific Expedition (2019QZKK0304). Jurek Müller, Qing Sun, and Fortunat Joos were supported by the Swiss National Science Foundation (#200020_200511). Qing Zhu and William Riley were supported by the Reducing Uncertainties in Biogeochemical Interactions through Synthesis and Computation (RUBISCO) Scientific Focus Area and Energy Exascale Earth System Modeling Project, which are sponsored by the Earth and Environmental Systems Modeling (EESM) program under the Office of Biological and Environmental Research of the U.S. Department of Energy Office of Science. Yuanzhi Yao and Hanqin Tian are funded in part by an NSF program (award number: #1903722) and the NASA CMS Program (award number: NX14AO73G). Tingting Li was supported by the National Key Scientific and Technological Infrastructure project "Earth System Science Numerical Simulator Facility" (EarthLab) and the Open Research Program of the International Research Center of Big Data for Sustainable Development Goals (grant no. CBAS2023ORP02). Peter Hopcroft was supported by a Birmingham Fellowship and the University of Birmingham's BlueBEAR high-performance computing (HPC) service. Wenxin Zhang acknowledges support from the LUNARC computation project LU 2021/2-114 and the Swedish Research Council (Vetenskapsrådet), starting grant 2020-05338. Wenxin Zhang and Paul A. Miller acknowledge this study as a contribution to the strategic research areas Modeling the Regional and Global Earth System (MERGE) and Biodiversity and Ecosystem Services in a Changing Climate (BECC) at Lund University. Robert B. Jackson acknowledges support from the United Nations Environment Programme (UNEP) to Stanford University DTIE21-EN3143. Nicola Gedney was supported by the Newton Fund through the Met Office Climate Science for Service Partnership Brazil (CSSP Brazil). Atul K. Jain and Xiaoming Xu were supported by the US National Science Foundation (NSF-831361857) and would like to acknowledge the high-performance computing support from Cheyenne (https://www.cisl.ucar.edu/ncar-supercomputing-history/cheyenne, last access: 15 January 2025, Cheyenne HPE, 2016), provided by NCAR's Computational and Information Systems Laboratory, sponsored by the National Science Foundation. Philippe Ciais acknowledges support from the space Agency Climate Change Initiative (ESA CCI) RECCAP2 project (grant no. ESRIN/4000123002/18/I-NB). Josep G. Canadell acknowledges the support of the Australian National Environmental Climate Science Program – Climate Systems hub. Gavin McNicol acknowledges support from the NASA CMS program (award number: NNH20ZDA001N).

Review statement. This paper was edited by Tyler Cyronak and reviewed by two anonymous referees.

References

Arndt, K. A., Oechel, W. C., Goodrich, J. P., Bailey, B. A., Kalhori, A., Hashemi, J., Sweeney, C., and Zona, D.: Sensitivity of Methane Emissions to Later Soil Freezing in Arctic

Tundra Ecosystems, J. Geophys. Res.-Biogeo., 124, 2595–2609, https://doi.org/10.1029/2019JG005242, 2019.

Arora, V. K., Melton, J. R., and Plummer, D.: An assessment of natural methane fluxes simulated by the CLASS-CTEM model, Biogeosciences, 15, 4683–4709, https://doi.org/10.5194/bg-15-4683-2018, 2018.

Bansal, S., Post van der Burg, M., Fern, R. R., Jones, J. W., Lo, R., McKenna, O. P., Tangen, B. A., Zhang, Z., and Gleason, R. A.: Large increases in methane emissions expected from North America's largest wetland complex, Sci. Adv., 9, eade1112, https://doi.org/10.1126/sciadv.ade1112, 2023.

Basso, L. S., Marani, L., Gatti, L. V., Miller, J. B., Gloor, M., Melack, J., Cassol, H. L. G., Tejada, G., Domingues, L. G., Arai, E., Sanchez, A. H., Corrêa, S. M., Anderson, L., Aragão, L. E. O. C., Correia, C. S. C., Crispim, S. P., and Neves, R. A. L.: Amazon methane budget derived from multi-year airborne observations highlights regional variations in emissions, Commun. Earth Environ., 2, 1–13, https://doi.org/10.1038/s43247-021-00314-4, 2021.

Bastviken, D., Treat, C. C., Pangala, S. R., Gauci, V., Enrich-Prast, A., Karlson, M., Gålfalk, M., Romano, M. B., and Sawakuchi, H. O.: The importance of plants for methane emission at the ecosystem scale, Aquat. Bot., 184, 103596, https://doi.org/10.1016/j.aquabot.2022.103596, 2023.

Basu, S., Lan, X., Dlugokencky, E., Michel, S., Schwietzke, S., Miller, J. B., Bruhwiler, L., Oh, Y., Tans, P. P., Apadula, F., Gatti, L. V., Jordan, A., Necki, J., Sasakawa, M., Morimoto, S., Di Iorio, T., Lee, H., Arduini, J., and Manca, G.: Estimating emissions of methane consistent with atmospheric measurements of methane and δ13C of methane, Atmos. Chem. Phys., 22, 15351–15377, https://doi.org/10.5194/acp-22-15351-2022, 2022.

Bergamaschi, P., Houweling, S., Segers, A., Krol, M., Frankenberg, C., Scheepmaker, R. A., Dlugokencky, E., Wofsy, S. C., Kort, E. A., Sweeney, C., Schuck, T., Brenninkmeijer, C., Chen, H., Beck, V., and Gerbig, C.: Atmospheric CH4 in the first decade of the 21st century: Inverse modeling analysis using SCIAMACHY satellite retrievals and NOAA surface measurements, J. Geophys. Res.-Atmos., 118, 7350–7369, https://doi.org/10.1002/jgrd.50480, 2013.

Bloom, A. A., Bowman, K. W., Lee, M., Turner, A. J., Schroeder, R., Worden, J. R., Weidner, R., McDonald, K. C., and Jacob, D. J.: A global wetland methane emissions and uncertainty dataset for atmospheric chemical transport models (WetCHARTs version 1.0), Geosci. Model Dev., 10, 2141–2156, https://doi.org/10.5194/gmd-10-2141-2017, 2017.

Boening, C., Willis, J. K., Landerer, F. W., Nerem, R. S., and Fasullo, J.: The 2011 La Niña: So strong, the oceans fell: La Niña 2011-SO strong, the oceans fell, Geophys. Res. Lett., 39, L19602, https://doi.org/10.1029/2012GL053055, 2012.

Bohn, T. J., Melton, J. R., Ito, A., Kleinen, T., Spahni, R., Stocker, B. D., Zhang, B., Zhu, X., Schroeder, R., Glagolev, M. V., Maksyutov, S., Brovkin, V., Chen, G., Denisov, S. N., Eliseev, A. V., Gallego-Sala, A., McDonald, K. C., Rawlins, M. A., Riley, W. J., Subin, Z. M., Tian, H., Zhuang, Q., and Kaplan, J. O.: WETCHIMP-WSL: intercomparison of wetland methane emissions models over West Siberia, Biogeosciences, 12, 3321–3349, https://doi.org/10.5194/bg-12-3321-2015, 2015.

Bousquet, P., Ciais, P., Miller, J. B., Dlugokencky, E. J., Hauglustaine, D. A., Prigent, C., Van der Werf, G. R., Peylin, P., Brunke, E.-G., Carouge, C., Langenfelds, R. L., Lathière, J., Papa, F., Ramonet, M., Schmidt, M., Steele, L. P., Tyler, S. C., and White, J.: Contribution of anthropogenic and natural sources to atmospheric methane variability, Nature, 443, 439–443, https://doi.org/10.1038/nature05132, 2006.

Bridgham, S. D., Cadillo-Quiroz, H., Keller, J. K., and Zhuang, Q.: Methane emissions from wetlands: biogeochemical, microbial, and modeling perspectives from local to global scales, Glob. Change Biol., 19, 1325–1346, https://doi.org/10.1111/gcb.12131, 2013.

Cao, M., Marshall, S., and Gregson, K.: Global carbon exchange and methane emissions from natural wetlands: Application of a process-based model, J. Geophys. Res.-Atmos., 101, 14399–14414, https://doi.org/10.1029/96JD00219, 1996.

Chang, K.-Y., Riley, W. J., Crill, P. M., Grant, R. F., and Saleska, S. R.: Hysteretic temperature sensitivity of wetland CH_4 fluxes explained by substrate availability and microbial activity, Biogeosciences, 17, 5849–5860, https://doi.org/10.5194/bg-17-5849-2020, 2020.

Chang, K.-Y., Riley, W. J., Knox, S. H., Jackson, R. B., McNicol, G., Poulter, B., Aurela, M., Baldocchi, D., Bansal, S., Bohrer, G., Campbell, D. I., Cescatti, A., Chu, H., Delwiche, K. B., Desai, A. R., Euskirchen, E., Friborg, T., Goeckede, M., Helbig, M., Hemes, K. S., Hirano, T., Iwata, H., Kang, M., Keenan, T., Krauss, K. W., Lohila, A., Mammarella, I., Mitra, B., Miyata, A., Nilsson, M. B., Noormets, A., Oechel, W. C., Papale, D., Peichl, M., Reba, M. L., Rinne, J., Runkle, B. R. K., Ryu, Y., Sachs, T., Schäfer, K. V. R., Schmid, H. P., Shurpali, N., Sonnentag, O., Tang, A. C. I., Torn, M. S., Trotta, C., Tuittila, E.-S., Ueyama, M., Vargas, R., Vesala, T., Windham-Myers, L., Zhang, Z., and Zona, D.: Substantial hysteresis in emergent temperature sensitivity of global wetland CH4 emissions, Nat. Commun., 12, 2266, https://doi.org/10.1038/s41467-021-22452-1, 2021.

Chang, K.-Y., Riley, W. J., Collier, N., McNicol, G., Fluet-Chouinard, E., Knox, S. H., Delwiche, K. B., Jackson, R. B., Poulter, B., Saunois, M., Chandra, N., Gedney, N., Ishizawa, M., Ito, A., Joos, F., Kleinen, T., Maggi, F., McNorton, J., Melton, J. R., Miller, P., Niwa, Y., Pasut, C., Patra, P. K., Peng, C., Peng, S., Segers, A., Tian, H., Tsuruta, A., Yao, Y., Yin, Y., Zhang, W., Zhang, Z., Zhu, Q., Zhu, Q., and Zhuang, Q.: Observational constraints reduce model spread but not uncertainty in global wetland methane emission estimates, Glob. Change Biol., 29, 4298–4312, https://doi.org/10.1111/gcb.16755, 2023.

Chang, R. Y.-W., Miller, C. E., Dinardo, S. J., Karion, A., Sweeney, C., Daube, B. C., Henderson, J. M., Mountain, M. E., Eluszkiewicz, J., Miller, J. B., Bruhwiler, L. M. P., and Wofsy, S. C.: Methane emissions from Alaska in 2012 from CARVE airborne observations, P. Natl. Acad. Sci. USA, 111, 16694–16699, https://doi.org/10.1073/pnas.1412953111, 2014.

Chu, H., Luo, X., Ouyang, Z., Chan, W. S., Dengel, S., Biraud, S. C., Torn, M. S., Metzger, S., Kumar, J., Arain, M. A., Arkebauer, T. J., Baldocchi, D., Bernacchi, C., Billesbach, D., Black, T. A., Blanken, P. D., Bohrer, G., Bracho, R., Brown, S., Brunsell, N. A., Chen, J., Chen, X., Clark, K., Desai, A. R., Duman, T., Durden, D., Fares, S., Forbrich, I., Gamon, J. A., Gough, C. M., Griffis, T., Helbig, M., Hollinger, D., Humphreys, E., Ikawa, H., Iwata, H., Ju, Y., Knowles, J. F., Knox, S. H., Kobayashi, H., Kolb, T., Law, B., Lee, X., Litvak, M., Liu, H., Munger, J. W., Noormets, A., Novick, K., Oberbauer, S.

F., Oechel, W., Oikawa, P., Papuga, S. A., Pendall, E., Prajapati, P., Prueger, J., Quinton, W. L., Richardson, A. D., Russell, E. S., Scott, R. L., Starr, G., Staebler, R., Stoy, P. C., Stuart-Haëntjens, E., Sonnentag, O., Sullivan, R. C., Suyker, A., Ueyama, M., Vargas, R., Wood, J. D., and Zona, D.: Representativeness of Eddy-Covariance flux footprints for areas surrounding AmeriFlux sites, Agr. Forest Meteorol., 301/302, 108350, https://doi.org/10.1016/j.agrformet.2021.108350, 2021.

Cucchi, M., Weedon, G. P., Amici, A., Bellouin, N., Lange, S., Müller Schmied, H., Hersbach, H., and Buontempo, C.: WFDE5: bias-adjusted ERA5 reanalysis data for impact studies, Earth Syst. Sci. Data, 12, 2097–2120, https://doi.org/10.5194/essd-12-2097-2020, 2020.

Delwiche, K. B., Knox, S. H., Malhotra, A., Fluet-Chouinard, E., McNicol, G., Feron, S., Ouyang, Z., Papale, D., Trotta, C., Canfora, E., Cheah, Y.-W., Christianson, D., Alberto, Ma. C. R., Alekseychik, P., Aurela, M., Baldocchi, D., Bansal, S., Billesbach, D. P., Bohrer, G., Bracho, R., Buchmann, N., Campbell, D. I., Celis, G., Chen, J., Chen, W., Chu, H., Dalmagro, H. J., Dengel, S., Desai, A. R., Detto, M., Dolman, H., Eichelmann, E., Euskirchen, E., Famulari, D., Fuchs, K., Goeckede, M., Gogo, S., Gondwe, M. J., Goodrich, J. P., Gottschalk, P., Graham, S. L., Heimann, M., Helbig, M., Helfter, C., Hemes, K. S., Hirano, T., Hollinger, D., Hörtnagl, L., Iwata, H., Jacotot, A., Jurasinski, G., Kang, M., Kasak, K., King, J., Klatt, J., Koebsch, F., Krauss, K. W., Lai, D. Y. F., Lohila, A., Mammarella, I., Belelli Marchesini, L., Manca, G., Matthes, J. H., Maximov, T., Merbold, L., Mitra, B., Morin, T. H., Nemitz, E., Nilsson, M. B., Niu, S., Oechel, W. C., Oikawa, P. Y., Ono, K., Peichl, M., Peltola, O., Reba, M. L., Richardson, A. D., Riley, W., Runkle, B. R. K., Ryu, Y., Sachs, T., Sakabe, A., Sanchez, C. R., Schuur, E. A., Schäfer, K. V. R., Sonnentag, O., Sparks, J. P., Stuart-Haëntjens, E., Sturtevant, C., Sullivan, R. C., Szutu, D. J., Thom, J. E., Torn, M. S., Tuittila, E.-S., Turner, J., Ueyama, M., Valach, A. C., Vargas, R., Varlagin, A., Vazquez-Lule, A., Verfaillie, J. G., Vesala, T., Vourlitis, G. L., Ward, E. J., Wille, C., Wohlfahrt, G., Wong, G. X., Zhang, Z., Zona, D., Windham-Myers, L., Poulter, B., and Jackson, R. B.: FLUXNET-CH4: a global, multi-ecosystem dataset and analysis of methane seasonality from freshwater wetlands , Earth Syst. Sci. Data, 13, 3607–3689, https://doi.org/10.5194/essd-13-3607-2021, 2021.

Dirmeyer, P. A., Gao, X., Zhao, M., Guo, Z., Oki, T., and Hanasaki, N.: GSWP-2: Multimodel Analysis and Implications for Our Perception of the Land Surface, Bull. Am. Meteorol. Soc., 87, 1381–1398, https://doi.org/10.1175/BAMS-87-10-1381, 2006.

Feng, L., Palmer, P. I., Zhu, S., Parker, R. J., and Liu, Y.: Tropical methane emissions explain large fraction of recent changes in global atmospheric methane growth rate, Nat. Commun., 13, 1378, https://doi.org/10.1038/s41467-022-28989-z, 2022.

Fleischmann, A. Papa, F., Hamilton, S. K., Fassoni-Andrade, A., Wongchuig, S., Espinoza, J., Paiva, R., Melack, J., Fluet-Chouinard, E., Castello, L., Almeida, R., Bonnet, M., Alves, L., Moreira, D., Yamazaki, D., Revel, M., and Collischonn, W.: Increased floodplain inundation in the Amazon since 1980, Environ. Res. Lett., 18, 034024, https://doi.org/10.1088/1748-9326/acb9a7, 2023.

Fluet-Chouinard, E., Stocker, B. D., Zhang, Z., Malhotra, A., Melton, J. R., Poulter, B., Kaplan, J. O., Goldewijk, K. K., Siebert, S., Minayeva, T., Hugelius, G., Joosten, H., Barthelmes, A., Prigent, C., Aires, F., Hoyt, A. M., Davidson, N., Finlayson, C. M., Lehner, B., Jackson, R. B., and McIntyre, P. B.: Extensive global wetland loss over the past three centuries, Nature, 614, 281–286, https://doi.org/10.1038/s41586-022-05572-6, 2023.

FLUXNET-CH4 Community Product: A global database of eddy covariance methane flux measurements, FLUXNET [data set], https://fluxnet.org/data/fluxnet-ch4-community-product/ (last access: 28 December 2024).

France, J. L., Lunt, M. F., Andrade, M., Moreno, I., Ganesan, A. L., Lachlan-Cope, T., Fisher, R. E., Lowry, D., Parker, R. J., Nisbet, E. G., and Jones, A. E.: Very large fluxes of methane measured above Bolivian seasonal wetlands, P. Natl. Acad. Sci. USA, 119, e2206345119, https://doi.org/10.1073/pnas.2206345119, 2022.

Gatti, L. V., Basso, L. S., Miller, J. B., Gloor, M., Gatti Domingues, L., Cassol, H. L. G., Tejada, G., Aragão, L. E. O. C., Nobre, C., Peters, W., Marani, L., Arai, E., Sanches, A. H., Corrêa, S. M., Anderson, L., Von Randow, C., Correia, C. S. C., Crispim, S. P., and Neves, R. A. L.: Amazonia as a carbon source linked to deforestation and climate change, Nature, 595, 388–393, https://doi.org/10.1038/s41586-021-03629-6, 2021.

Gedney, N.: Climate feedback from wetland methane emissions, Geophys. Res. Lett., 31, L20503, https://doi.org/10.1029/2004GL020919, 2004.

Gerlein-Safdi, C., Bloom, A. A., Plant, G., Kort, E. A., and Ruf, C. S.: Improving Representation of Tropical Wetland Methane Emissions With CYGNSS Inundation Maps, Global Biogeochem. Cy., 35, e2020GB006890, https://doi.org/10.1029/2020GB006890, 2021.

Glagolev, M., Kleptsova, I., Filippov, I., Maksyutov, S., and Machida, T.: Regional methane emission from West Siberia mire landscapes, Environ. Res. Lett., 6, 045214, https://doi.org/10.1088/1748-9326/6/4/045214, 2011.

Gloor, M., Gatti, L. V., Wilson, C., Parker, R. J., Boesch, H., Popa, E., Chipperfield, M. P., Poulter, B., Zhang, Z., Basso, L., Miller, J., McNorton, J., Jimenez, C., and Prigent, C.: Large Methane Emissions From the Pantanal During Rising Water-Levels Revealed by Regularly Measured Lower Troposphere CH4 Profiles, Global Biogeochem. Cy., 35, e2021GB006964, https://doi.org/10.1029/2021GB006964, 2021.

Grant, R. F., Mekonnen, Z. A., Riley, W. J., Arora, B., and Torn, M. S.: Mathematical Modelling of Arctic Polygonal Tundra with Ecosys: 2. Microtopography Determines How CO_2 and CH_4 Exchange Responds to Changes in Temperature and Precipitation, J. Geophys. Res.-Biogeo., 122, 3174–3187, https://doi.org/10.1002/2017JG004037, 2017.

Harris, I., Jones, P. D., Osborn, T. J., and Lister, D. H.: Updated high-resolution grids of monthly climatic observations – the CRU TS3.10 Dataset: updated high-resolution grids of monthly climatic observations, Int. J. Climatol., 34, 623–642, https://doi.org/10.1002/joc.3711, 2014.

Hopcroft, P. O., Valdes, P. J., O'Connor, F. M., Kaplan, J. O., and Beerling, D. J.: Understanding the glacial methane cycle, Nat. Commun., 8, 14383, https://doi.org/10.1038/ncomms14383, 2017.

Kaiser, S., Göckede, M., Castro-Morales, K., Knoblauch, C., Ekici, A., Kleinen, T., Zubrzycki, S., Sachs, T., Wille, C., and Beer, C.: Process-based modelling of the methane balance in periglacial landscapes (JSBACH-methane), Geosci. Model Dev., 10, 333–358, https://doi.org/10.5194/gmd-10-333-2017, 2017.

Kirschke, S., Bousquet, P., Ciais, P., Saunois, M., Canadell, J. G., Dlugokencky, E. J., Bergamaschi, P., Bergmann, D., Blake, D. R., Bruhwiler, L., Cameron-Smith, P., Castaldi, S., Chevallier, F., Feng, L., Fraser, A., Heimann, M., Hodson, E. L., Houweling, S., Josse, B., Fraser, P. J., Krummel, P. B., Lamarque, J.-F., Langenfelds, R. L., Le Quéré, C., Naik, V., O'Doherty, S., Palmer, P. I., Pison, I., Plummer, D., Poulter, B., Prinn, R. G., Rigby, M., Ringeval, B., Santini, M., Schmidt, M., Shindell, D. T., Simpson, I. J., Spahni, R., Steele, L. P., Strode, S. A., Sudo, K., Szopa, S., van der Werf, G. R., Voulgarakis, A., van Weele, M., Weiss, R. F., Williams, J. E., and Zeng, G.: Three decades of global methane sources and sinks, Nat. Geosci., 6, 813–823, https://doi.org/10.1038/ngeo1955, 2013.

Kleinen, T., Gromov, S., Steil, B., and Brovkin, V.: Atmospheric methane since the last glacial maximum was driven by wetland sources, Clim. Past, 19, 1081–1099, https://doi.org/10.5194/cp-19-1081-2023, 2023.

Knox, S. H., Jackson, R. B., Poulter, B., McNicol, G., Fluet-Chouinard, E., Zhang, Z., Hugelius, G., Bousquet, P., Canadell, J. G., Saunois, M., Papale, D., Chu, H., Keenan, T. F., Baldocchi, D., Torn, M. S., Mammarella, I., Trotta, C., Aurela, M., Bohrer, G., Campbell, D. I., Cescatti, A., Chamberlain, S., Chen, J., Chen, W., Dengel, S., Desai, A. R., Euskirchen, E., Friborg, T., Gasbarra, D., Goded, I., Goeckede, M., Heimann, M., Helbig, M., Hirano, T., Hollinger, D. Y., Iwata, H., Kang, M., Klatt, J., Krauss, K. W., Kutzbach, L., Lohila, A., Mitra, B., Morin, T. H., Nilsson, M. B., Niu, S., Noormets, A., Oechel, W. C., Peichl, M., Peltola, O., Reba, M. L., Richardson, A. D., Runkle, B. R. K., Ryu, Y., Sachs, T., Schäfer, K. V. R., Schmid, H. P., Shurpali, N., Sonnentag, O., Tang, A. C. I., Ueyama, M., Vargas, R., Vesala, T., Ward, E. J., Windham-Myers, L., Wohlfahrt, G., and Zona, D.: FLUXNET-CH_4 Synthesis Activity: Objectives, Observations, and Future Directions, Bull. Am. Meteorol. Soc., 100, 2607–2632, https://doi.org/10.1175/BAMS-D-18-0268.1, 2019.

Koffi, E. N., Bergamaschi, P., Alkama, R., and Cescatti, A.: An observation-constrained assessment of the climate sensitivity and future trajectories of wetland methane emissions, Sci. Adv., 6, eaay4444, https://doi.org/10.1126/sciadv.aay4444, 2020.

Kuhn, M. A., Varner, R. K., Bastviken, D., Crill, P., MacIntyre, S., Turetsky, M., Walter Anthony, K., McGuire, A. D., and Olefeldt, D.: BAWLD-CH_4: a comprehensive dataset of methane fluxes from boreal and arctic ecosystems, Earth Syst. Sci. Data, 13, 5151–5189, https://doi.org/10.5194/essd-13-5151-2021, 2021.

Li, M., Kort, E. A., Bloom, A. A., Wu, D., Plant, G., Gerlein-Safdi, C., and Pu, T.: Underestimated Dry Season Methane Emissions from Wetlands in the Pantanal, Environ. Sci. Technol., 58, 3278–3287, https://doi.org/10.1021/acs.est.3c09250, 2024.

Lan, X., Basu, S., Schwietzke, S., Bruhwiler, L. M. P., Dlugokencky, E. J., Michel, S. E., Sherwood, O. A., Tans, P. P., Thoning, K., Etiope, G., Zhuang, Q., Liu, L., Oh, Y., Miller, J. B., Pétron, G., Vaughn, B. H., and Crippa, M.: Improved Constraints on Global Methane Emissions and Sinks Using δ^{13}C-CH_4, Global Biogeochem. Cy., 35, e2021GB007000, https://doi.org/10.1029/2021GB007000, 2021.

Lunt, M. F., Palmer, P. I., Lorente, A., Borsdorff, T., Landgraf, J., Parker, R. J., and Boesch, H.: Rain-fed pulses of methane from East Africa during 2018–2019 contributed to atmospheric growth rate, Environ. Res. Lett., 16, 024021, https://doi.org/10.1088/1748-9326/abd8fa, 2021.

Mahecha, M. D., Reichstein, M., Carvalhais, N., Lasslop, G., Lange, H., Seneviratne, S. I., Vargas, R., Ammann, C., Arain, M. A., Cescatti, A., Janssens, I. A., Migliavacca, M., Montagnani, L., and Richardson, A. D.: Global Convergence in the Temperature Sensitivity of Respiration at Ecosystem Level, Science, 329, 838–840, https://doi.org/10.1126/science.1189587, 2010.

Mastepanov, M., Sigsgaard, C., Dlugokencky, E. J., Houweling, S., Ström, L., Tamstorf, M. P., and Christensen, T. R.: Large tundra methane burst during onset of freezing, Nature, 456, 628–630, https://doi.org/10.1038/nature07464, 2008.

McNicol, G., Fluet-Chouinard, E., Ouyang, Z., Knox, S., Zhang, Z., Aalto, T., Bansal, S., Chang, K.-Y., Chen, M., Delwiche, K., Feron, S., Goeckede, M., Liu, J., Malhotra, A., Melton, J. R., Riley, W., Vargas, R., Yuan, K., Ying, Q., Zhu, Q., Alekseychik, P., Aurela, M., Billesbach, D. P., Campbell, D. I., Chen, J., Chu, H., Desai, A. R., Euskirchen, E., Goodrich, J., Griffis, T., Helbig, M., Hirano, T., Iwata, H., Jurasinski, G., King, J., Koebsch, F., Kolka, R., Krauss, K., Lohila, A., Mammarella, I., Nilson, M., Noormets, A., Oechel, W., Peichl, M., Sachs, T., Sakabe, A., Schulze, C., Sonnentag, O., Sullivan, R. C., Tuittila, E.-S., Ueyama, M., Vesala, T., Ward, E., Wille, C., Wong, G. X., Zona, D., Windham-Myers, L., Poulter, B., and Jackson, R. B.: Upscaling Wetland Methane Emissions From the FLUXNET-CH4 Eddy Covariance Network (UpCH4 v1.0): Model Development, Network Assessment, and Budget Comparison, AGU Advances, 4, e2023AV000956, https://doi.org/10.1029/2023AV000956, 2023.

Meinshausen, M., Vogel, E., Nauels, A., Lorbacher, K., Meinshausen, N., Etheridge, D. M., Fraser, P. J., Montzka, S. A., Rayner, P. J., Trudinger, C. M., Krummel, P. B., Beyerle, U., Canadell, J. G., Daniel, J. S., Enting, I. G., Law, R. M., Lunder, C. R., O'Doherty, S., Prinn, R. G., Reimann, S., Rubino, M., Velders, G. J. M., Vollmer, M. K., Wang, R. H. J., and Weiss, R.: Historical greenhouse gas concentrations for climate modelling (CMIP6), Geosci. Model Dev., 10, 2057–2116, https://doi.org/10.5194/gmd-10-2057-2017, 2017.

Melton, J. R., Wania, R., Hodson, E. L., Poulter, B., Ringeval, B., Spahni, R., Bohn, T., Avis, C. A., Beerling, D. J., Chen, G., Eliseev, A. V., Denisov, S. N., Hopcroft, P. O., Lettenmaier, D. P., Riley, W. J., Singarayer, J. S., Subin, Z. M., Tian, H., Zürcher, S., Brovkin, V., van Bodegom, P. M., Kleinen, T., Yu, Z. C., and Kaplan, J. O.: Present state of global wetland extent and wetland methane modelling: conclusions from a model intercomparison project (WETCHIMP), Biogeosciences, 10, 753–788, https://doi.org/10.5194/bg-10-753-2013, 2013.

Miller, S. M., Miller, C. E., Commane, R., Chang, R. Y.-W., Dinardo, S. J., Henderson, J. M., Karion, A., Lindaas, J., Melton, J. R., Miller, J. B., Sweeney, C., Wofsy, S. C., and Michalak, A. M.: A multiyear estimate of methane fluxes in Alaska from CARVE atmospheric observations: METHANE FLUXES FROM ALASKA, Global Biogeochem. Cy., 30, 1441–1453, https://doi.org/10.1002/2016GB005419, 2016.

Natali, S. M., Watts, J. D., Rogers, B. M., Potter, S., Ludwig, S. M., Selbmann, A.-K., Sullivan, P. F., Abbott, B. W., Arndt, K. A., Birch, L., Björkman, M. P., Bloom, A. A., Celis, G., Christensen, T. R., Christiansen, C. T., Commane, R., Cooper, E. J., Crill, P., Czimczik, C., Davydov, S., Du, J., Egan, J. E., Elberling, B., Euskirchen, E. S., Friborg, T., Genet, H., Göckede, M., Goodrich, J. P., Grogan, P., Helbig, M., Jafarov, E. E., Jastrow, J. D., Kalhori, A. A. M., Kim, Y., Kimball, J. S., Kutzbach, L.,

Lara, M. J., Larsen, K. S., Lee, B.-Y., Liu, Z., Loranty, M. M., Lund, M., Lupascu, M., Madani, N., Malhotra, A., Matamala, R., McFarland, J., McGuire, A. D., Michelsen, A., Minions, C., Oechel, W. C., Olefeldt, D., Parmentier, F.-J. W., Pirk, N., Poulter, B., Quinton, W., Rezanezhad, F., Risk, D., Sachs, T., Schaefer, K., Schmidt, N. M., Schuur, E. A. G., Semenchuk, P. R., Shaver, G., Sonnentag, O., Starr, G., Treat, C. C., Waldrop, M. P., Wang, Y., Welker, J., Wille, C., Xu, X., Zhang, Z., Zhuang, Q., and Zona, D.: Large loss of CO_2 in winter observed across the northern permafrost region, Nat. Clim. Change, 9, 852–857, https://doi.org/10.1038/s41558-019-0592-8, 2019.

Nisbet, E. G., Manning, M. R., Dlugokencky, E. J., Fisher, R. E., Lowry, D., Michel, S. E., Myhre, C. L., Platt, S. M., Allen, G., Bousquet, P., Brownlow, R., Cain, M., France, J. L., Hermansen, O., Hossaini, R., Jones, A. E., Levin, I., Manning, A. C., Myhre, G., Pyle, J. A., Vaughn, B. H., Warwick, N. J., and White, J. W. C.: Very Strong Atmospheric Methane Growth in the 4 Years 2014–2017: Implications for the Paris Agreement, Global Biogeochem. Cy., 33, 318–342, https://doi.org/10.1029/2018GB006009, 2019.

Nisbet, E. G., Manning, M. R., Dlugokencky, E. J., Michel, S. E., Lan, X., Röckmann, T., Denier van der Gon, H. A. C., Schmitt, J., Palmer, P. I., Dyonisius, M. N., Oh, Y., Fisher, R. E., Lowry, D., France, J. L., White, J. W. C., Brailsford, G., and Bromley, T.: Atmospheric Methane: Comparison Between Methane's Record in 2006–2022 and During Glacial Terminations, Global Biogeochem. Cy., 37, e2023GB007875, https://doi.org/10.1029/2023GB007875, 2023.

Palmer, P. I., Woodwark, A. J. P., Finch, D. P., Taylor, T. E., Butz, A., Tamminen, J., Bösch, H., Eldering, A., and Vincent-Bonnieu, S.: Role of space station instruments for improving tropical carbon flux estimates using atmospheric data, npj Microgravity, 8, 51, https://doi.org/10.1038/s41526-022-00231-6, 2022.

Pandey, S., Houweling, S., Lorente, A., Borsdorff, T., Tsivlidou, M., Bloom, A. A., Poulter, B., Zhang, Z., and Aben, I.: Using satellite data to identify the methane emission controls of South Sudan's wetlands, Biogeosciences, 18, 557–572, https://doi.org/10.5194/bg-18-557-2021, 2021.

Parker, R. J., Wilson, C., Bloom, A. A., Comyn-Platt, E., Hayman, G., McNorton, J., Boesch, H., and Chipperfield, M. P.: Exploring constraints on a wetland methane emission ensemble (WetCHARTs) using GOSAT observations, Biogeosciences, 17, 5669–5691, https://doi.org/10.5194/bg-17-5669-2020, 2020.

Patra, P. K., Houweling, S., Krol, M., Bousquet, P., Belikov, D., Bergmann, D., Bian, H., Cameron-Smith, P., Chipperfield, M. P., Corbin, K., Fortems-Cheiney, A., Fraser, A., Gloor, E., Hess, P., Ito, A., Kawa, S. R., Law, R. M., Loh, Z., Maksyutov, S., Meng, L., Palmer, P. I., Prinn, R. G., Rigby, M., Saito, R., and Wilson, C.: TransCom model simulations of CH_4 and related species: linking transport, surface flux and chemical loss with CH_4 variability in the troposphere and lower stratosphere, Atmos. Chem. Phys., 11, 12813–12837, https://doi.org/10.5194/acp-11-12813-2011, 2011.

Peng, S., Lin, X., Thompson, R. L., Xi, Y., Liu, G., Hauglustaine, D., Lan, X., Poulter, B., Ramonet, M., Saunois, M., Yin, Y., Zhang, Z., Zheng, B., and Ciais, P.: Wetland emission and atmospheric sink changes explain methane growth in 2020, Nature, 612, 477–482, https://doi.org/10.1038/s41586-022-05447-w, 2022.

Petrescu, A. M. R., van Beek, L. P. H., van Huissteden, J., Prigent, C., Sachs, T., Corradi, C. A. R., Parmentier, F. J. W., and Dolman, A. J.: Modeling regional to global CH_4 emissions of boreal and arctic wetlands: Modeling Global CH_4 Emissions, Global Biogeochem. Cy., 24, GB4009, https://doi.org/10.1029/2009GB003610, 2010.

Piao, S., Sitch, S., Ciais, P., Friedlingstein, P., Peylin, P., Wang, X., Ahlström, A., Anav, A., Canadell, J. G., Cong, N., Huntingford, C., Jung, M., Levis, S., Levy, P. E., Li, J., Lin, X., Lomas, M. R., Lu, M., Luo, Y., Ma, Y., Myneni, R. B., Poulter, B., Sun, Z., Wang, T., Viovy, N., Zaehle, S., and Zeng, N.: Evaluation of terrestrial carbon cycle models for their response to climate variability and to CO_2 trends, Glob. Change Biol., 19, 2117–2132, https://doi.org/10.1111/gcb.12187, 2013.

Pickett-Heaps, C. A., Jacob, D. J., Wecht, K. J., Kort, E. A., Wofsy, S. C., Diskin, G. S., Worthy, D. E. J., Kaplan, J. O., Bey, I., and Drevet, J.: Magnitude and seasonality of wetland methane emissions from the Hudson Bay Lowlands (Canada), Atmos. Chem. Phys., 11, 3773–3779, https://doi.org/10.5194/acp-11-3773-2011, 2011.

Poulter, B., Bousquet, P., Canadell, J. G., Ciais, P., Peregon, A., Saunois, M., Arora, V. K., Beerling, D. J., Brovkin, V., Jones, C. D., Joos, F., Gedney, N., Ito, A., Kleinen, T., Koven, C. D., McDonald, K., Melton, J. R., Peng, C., Peng, S., Prigent, C., Schroeder, R., Riley, W. J., Saito, M., Spahni, R., Tian, H., Taylor, L., Viovy, N., Wilton, D., Wiltshire, A., Xu, X., Zhang, B., Zhang, Z., and Zhu, Q.: Global wetland contribution to 2000–2012 atmospheric methane growth rate dynamics, Environ. Res. Lett., 12, 094013, https://doi.org/10.1088/1748-9326/aa8391, 2017.

Prigent, C., Jimenez, C., and Bousquet, P.: Satellite-Derived Global Surface Water Extent and Dynamics Over the Last 25 Years (GIEMS-2), J. Geophys. Res.-Atmos., 125, e2019JD030711, https://doi.org/10.1029/2019JD030711, 2020.

Qu, Z., Jacob, D. J., Zhang, Y., Shen, L., Varon, D. J., Lu, X., Scarpelli, T., Bloom, A., Worden, J., and Parker, R. J.: Attribution of the 2020 surge in atmospheric methane by inverse analysis of GOSAT observations, Environ. Res. Lett., 17, 094003, https://doi.org/10.1088/1748-9326/ac8754, 2022.

Ringeval, B., Houweling, S., van Bodegom, P. M., Spahni, R., van Beek, R., Joos, F., and Röckmann, T.: Methane emissions from floodplains in the Amazon Basin: challenges in developing a process-based model for global applications, Biogeosciences, 11, 1519–1558, https://doi.org/10.5194/bg-11-1519-2014, 2014.

Rößger, N., Sachs, T., Wille, C., Boike, J., and Kutzbach, L.: Seasonal increase of methane emissions linked to warming in Siberian tundra, Nat. Clim. Change, 12, 1031–1036, https://doi.org/10.1038/s41558-022-01512-4, 2022.

Saunois, M., Bousquet, P., Poulter, B., Peregon, A., Ciais, P., Canadell, J. G., Dlugokencky, E. J., Etiope, G., Bastviken, D., Houweling, S., Janssens-Maenhout, G., Tubiello, F. N., Castaldi, S., Jackson, R. B., Alexe, M., Arora, V. K., Beerling, D. J., Bergamaschi, P., Blake, D. R., Brailsford, G., Brovkin, V., Bruhwiler, L., Crevoisier, C., Crill, P., Covey, K., Curry, C., Frankenberg, C., Gedney, N., Höglund-Isaksson, L., Ishizawa, M., Ito, A., Joos, F., Kim, H.-S., Kleinen, T., Krummel, P., Lamarque, J.-F., Langenfelds, R., Locatelli, R., Machida, T., Maksyutov, S., McDonald, K. C., Marshall, J., Melton, J. R., Morino, I., Naik, V., O'Doherty, S., Parmentier, F.-J. W., Patra, P. K., Peng, C., Peng, S., Peters,

G. P., Pison, I., Prigent, C., Prinn, R., Ramonet, M., Riley, W. J., Saito, M., Santini, M., Schroeder, R., Simpson, I. J., Spahni, R., Steele, P., Takizawa, A., Thornton, B. F., Tian, H., Tohjima, Y., Viovy, N., Voulgarakis, A., van Weele, M., van der Werf, G. R., Weiss, R., Wiedinmyer, C., Wilton, D. J., Wiltshire, A., Worthy, D., Wunch, D., Xu, X., Yoshida, Y., Zhang, B., Zhang, Z., and Zhu, Q.: The Global Methane Budget 2000–2012, Earth Syst. Sci. Data, 8, 697–751, https://doi.org/10.5194/essd-8-697-2016, 2016.

Saunois, M., Stavert, A. R., Poulter, B., Bousquet, P., Canadell, J. G., Jackson, R. B., Raymond, P. A., Dlugokencky, E. J., Houweling, S., Patra, P. K., Ciais, P., Arora, V. K., Bastviken, D., Bergamaschi, P., Blake, D. R., Brailsford, G., Bruhwiler, L., Carlson, K. M., Carrol, M., Castaldi, S., Chandra, N., Crevoisier, C., Crill, P. M., Covey, K., Curry, C. L., Etiope, G., Frankenberg, C., Gedney, N., Hegglin, M. I., Höglund-Isaksson, L., Hugelius, G., Ishizawa, M., Ito, A., Janssens-Maenhout, G., Jensen, K. M., Joos, F., Kleinen, T., Krummel, P. B., Langenfelds, R. L., Laruelle, G. G., Liu, L., Machida, T., Maksyutov, S., McDonald, K. C., McNorton, J., Miller, P. A., Melton, J. R., Morino, I., Müller, J., Murguia-Flores, F., Naik, V., Niwa, Y., Noce, S., O'Doherty, S., Parker, R. J., Peng, C., Peng, S., Peters, G. P., Prigent, C., Prinn, R., Ramonet, M., Regnier, P., Riley, W. J., Rosentreter, J. A., Segers, A., Simpson, I. J., Shi, H., Smith, S. J., Steele, L. P., Thornton, B. F., Tian, H., Tohjima, Y., Tubiello, F. N., Tsuruta, A., Viovy, N., Voulgarakis, A., Weber, T. S., van Weele, M., van der Werf, G. R., Weiss, R. F., Worthy, D., Wunch, D., Yin, Y., Yoshida, Y., Zhang, W., Zhang, Z., Zhao, Y., Zheng, B., Zhu, Q., Zhu, Q., and Zhuang, Q.: The Global Methane Budget 2000–2017, Earth Syst. Sci. Data, 12, 1561–1623, https://doi.org/10.5194/essd-12-1561-2020, 2020.

Schaefer, K., Schwalm, C. R., Williams, C., Arain, M. A., Barr, A., Chen, J. M., Davis, K. J., Dimitrov, D., Hilton, T. W., Hollinger, D. Y., Humphreys, E., Poulter, B., Raczka, B. M., Richardson, A. D., Sahoo, A., Thornton, P., Vargas, R., Verbeeck, H., Anderson, R., Baker, I., Black, T. A., Bolstad, P., Chen, J., Curtis, P. S., Desai, A. R., Dietze, M., Dragoni, D., Gough, C., Grant, R. F., Gu, L., Jain, A., Kucharik, C., Law, B., Liu, S., Lokipitiya, E., Margolis, H. A., Matamala, R., McCaughey, J. H., Monson, R., Munger, J. W., Oechel, W., Peng, C., Price, D. T., Ricciuto, D., Riley, W. J., Roulet, N., Tian, H., Tonitto, C., Torn, M., Weng, E., and Zhou, X.: A model-data comparison of gross primary productivity: Results from the North American Carbon Program site synthesis, J. Geophys. Res.-Biogeo., 117, G03010, https://doi.org/10.1029/2012JG001960, 2012.

Schaefer, H., Fletcher, S. E. M., Veidt, C., Lassey, K. R., Brailsford, G. W., Bromley, T. M., Dlugokencky, E. J., Michel, S. E., Miller, J. B., Levin, I., Lowe, D. C., Martin, R. J., Vaughn, B. H., and White, J. W. C.: A 21st-century shift from fossil-fuel to biogenic methane emissions indicated by 13CH4, Science, 352, 80–84, https://doi.org/10.1126/science.aad2705, 2016.

Shaw, J. T., Allen, G., Barker, P., Pitt, J. R., Pasternak, D., Bauguitte, S. J.-B., Lee, J., Bower, K. N., Daly, M. C., Lunt, M. F., Ganesan, A. L., Vaughan, A. R., Chibesakunda, F., Lambakasa, M., Fisher, R. E., France, J. L., Lowry, D., Palmer, P. I., Metzger, S., Parker, R. J., Gedney, N., Bateson, P., Cain, M., Lorente, A., Borsdorff, T., and Nisbet, E. G.: Large Methane Emission Fluxes Observed From Tropical Wetlands in Zambia, Global Biogeochem. Cy., 36, e2021GB007261, https://doi.org/10.1029/2021GB007261, 2022.

Shindell, D. and Smith, C. J.: Climate and air-quality benefits of a realistic phase-out of fossil fuels, Nature, 573, 408–411, https://doi.org/10.1038/s41586-019-1554-z, 2019.

Shu, S., Jain, A. K., and Kheshgi, H. S.: Investigating Wetland and Nonwetland Soil Methane Emissions and Sinks Across the Contiguous United States Using a Land Surface Model, Global Biogeochem. Cy., 34, e2019GB006251, https://doi.org/10.1029/2019GB006251, 2020.

Spahni, R., Wania, R., Neef, L., van Weele, M., Pison, I., Bousquet, P., Frankenberg, C., Foster, P. N., Joos, F., Prentice, I. C., and van Velthoven, P.: Constraining global methane emissions and uptake by ecosystems, Biogeosciences, 8, 1643–1665, https://doi.org/10.5194/bg-8-1643-2011, 2011.

Sun, Q., Miao, C., Duan, Q., Ashouri, H., Sorooshian, S., and Hsu, K.-L.: A Review of Global Precipitation Data Sets: Data Sources, Estimation, and Intercomparisons, Rev. Geophys., 56, 79–107, https://doi.org/10.1002/2017RG000574, 2018.

Treat, C. C., Bloom, A. A., and Marushchak, M. E.: Nongrowing season methane emissions-a significant component of annual emissions across northern ecosystems, Glob. Change Biol., 24, 3331–3343, https://doi.org/10.1111/gcb.14137, 2018.

Tunnicliffe, R. L., Ganesan, A. L., Parker, R. J., Boesch, H., Gedney, N., Poulter, B., Zhang, Z., Lavrič, J. V., Walter, D., Rigby, M., Henne, S., Young, D., and O'Doherty, S.: Quantifying sources of Brazil's CH4 emissions between 2010 and 2018 from satellite data, Atmos. Chem. Phys., 20, 13041–13067, https://doi.org/10.5194/acp-20-13041-2020, 2020.

van Groenigen, K. J., Osenberg, C. W., and Hungate, B. A.: Increased soil emissions of potent greenhouse gases under increased atmospheric CO_2, Nature, 475, 214–216, https://doi.org/10.1038/nature10176, 2011.

Wania, R., Melton, J. R., Hodson, E. L., Poulter, B., Ringeval, B., Spahni, R., Bohn, T., Avis, C. A., Chen, G., Eliseev, A. V., Hopcroft, P. O., Riley, W. J., Subin, Z. M., Tian, H., van Bodegom, P. M., Kleinen, T., Yu, Z. C., Singarayer, J. S., Zürcher, S., Lettenmaier, D. P., Beerling, D. J., Denisov, S. N., Prigent, C., Papa, F., and Kaplan, J. O.: Present state of global wetland extent and wetland methane modelling: methodology of a model inter-comparison project (WETCHIMP), Geosci. Model Dev., 6, 617–641, https://doi.org/10.5194/gmd-6-617-2013, 2013.

Wilson, C., Gloor, M., Gatti, L. V., Miller, J. B., Monks, S. A., McNorton, J., Bloom, A. A., Basso, L. S., and Chipperfield, M. P.: Contribution of regional sources to atmospheric methane over the Amazon Basin in 2010 and 2011: REGIONAL CH_4 SOURCES IN THE AMAZON BASIN, Global Biogeochem. Cy., 30, 400–420, https://doi.org/10.1002/2015GB005300, 2016.

Wilson, C., Chipperfield, M. P., Gloor, M., Parker, R. J., Boesch, H., McNorton, J., Gatti, L. V., Miller, J. B., Basso, L. S., and Monks, S. A.: Large and increasing methane emissions from eastern Amazonia derived from satellite data, 2010–2018, Atmos. Chem. Phys., 21, 10643–10669, https://doi.org/10.5194/acp-21-10643-2021, 2021.

Xi, Y., Peng, S., Ducharne, A., Ciais, P., Gumbricht, T., Jimenez, C., Poulter, B., Prigent, C., Qiu, C., Saunois, M., and Zhang, Z.: Gridded maps of wetlands dynamics over mid-low latitudes for 1980–2020 based on TOPMODEL, Sci. Data, 9, 347, https://doi.org/10.1038/s41597-022-01460-w, 2022.

Yin, Y., Chevallier, F., Ciais, P., Bousquet, P., Saunois, M., Zheng, B., Worden, J., Bloom, A. A., Parker, R. J., Jacob, D. J., Dlugokencky, E. J., and Frankenberg, C.: Accelerating methane growth rate from 2010 to 2017: leading contributions from the tropics and East Asia, Atmos. Chem. Phys., 21, 12631–12647, https://doi.org/10.5194/acp-21-12631-2021, 2021.

Ying, Q., Poulter, B., Watts, J. D., Arndt, K. A., Virkkala, A.-M., Bruhwiler, L., Oh, Y., Rogers, B. M., Natali, S. M., Sullivan, H., Schiferl, L. D., Elder, C., Peltola, O., Bartsch, A., Armstrong, A., Desai, A. R., Euskirchen, E., Göckede, M., Lehner, B., Nilsson, M. B., Peichl, M., Sonnentag, O., Tuittila, E.-S., Sachs, T., Kalhori, A., Ueyama, M., and Zhang, Z.: WetCH4: A Machine Learning-based Upscaling of Methane Fluxes of Northern Wetlands during 2016–2022, Earth Syst. Sci. Data Discuss. [preprint], https://doi.org/10.5194/essd-2024-84, in review, 2024.

Yuan, K., Li, F., McNicol, G., Chen, M., Hoyt, A., Knox, S., Riley, W. J., Jackson, R., and Zhu, Q.: Boreal–Arctic wetland methane emissions modulated by warming and vegetation activity, Nat. Clim. Change, 14, 282–288, https://doi.org/10.1038/s41558-024-01933-3, 2024.

Yvon-Durocher, G., Allen, A. P., Bastviken, D., Conrad, R., Gudasz, C., St-Pierre, A., Thanh-Duc, N., and del Giorgio, P. A.: Methane fluxes show consistent temperature dependence across microbial to ecosystem scales, Nature, 507, 488–491, https://doi.org/10.1038/nature13164, 2014.

Zhang, Y., Jacob, D. J., Lu, X., Maasakkers, J. D., Scarpelli, T. R., Sheng, J.-X., Shen, L., Qu, Z., Sulprizio, M. P., Chang, J., Bloom, A. A., Ma, S., Worden, J., Parker, R. J., and Boesch, H.: Attribution of the accelerating increase in atmospheric methane during 2010–2018 by inverse analysis of GOSAT observations, Atmos. Chem. Phys., 21, 3643–3666, https://doi.org/10.5194/acp-21-3643-2021, 2021b.

Zhang, Z.: Ensemble estimate of global Wetland Methane (CH_4) Emissions (2000–2020), Zenodo [data set], https://doi.org/10.5281/zenodo.11309188, 2024.

Zhang, Z., Zimmermann, N. E., Stenke, A., Li, X., Hodson, E. L., Zhu, G., Huang, C., and Poulter, B.: Emerging role of wetland methane emissions in driving 21st century climate change, P. Natl. Acad. Sci. USA, 114, 9647–9652, https://doi.org/10.1073/pnas.1618765114, 2017.

Zhang, Z., Zimmermann, N. E., Calle, L., Hurtt, G., Chatterjee, A., and Poulter, B.: Enhanced response of global wetland methane emissions to the 2015–2016 El Niño-Southern Oscillation event, Environ. Res. Lett., 13, 074009, https://doi.org/10.1088/1748-9326/aac939, 2018.

Zhang, Z., Fluet-Chouinard, E., Jensen, K., McDonald, K., Hugelius, G., Gumbricht, T., Carroll, M., Prigent, C., Bartsch, A., and Poulter, B.: Development of the global dataset of Wetland Area and Dynamics for Methane Modeling (WAD2M), Earth Syst. Sci. Data, 13, 2001–2023, https://doi.org/10.5194/essd-13-2001-2021, 2021a.

Zhang, Z., Poulter, B., Knox, S., Stavert, A., McNicol, G., Fluet-Chouinard, E., Feinberg, A., Zhao, Y., Bousquet, P., Canadell, J. G., Ganesan, A., Hugelius, G., Hurtt, G., Jackson, R. B., Patra, P. K., Saunois, M., Höglund-Isaksson, L., Huang, C., Chatterjee, A., and Li, X.: Anthropogenic emission is the main contributor to the rise of atmospheric methane during 1993–2017, Nat. Sci. Rev., 9, nwab200, https://doi.org/10.1093/nsr/nwab200, 2021c.

Zhang, Z., Poulter, B., Feldman, A. F., Ying, Q., Ciais, P., Peng, S., and Li, X.: Recent intensification of wetland methane feedback, Nat. Clim. Change, 13, 430–433, https://doi.org/10.1038/s41558-023-01629-0, 2023a.

Zhang, Z., Bansal, S., Chang, K.-Y., Fluet-Chouinard, E., Delwiche, K., Goeckede, M., Gustafson, A., Knox, S., Leppänen, A., Liu, L., Liu, J., Malhotra, A., Markkanen, T., McNicol, G., Melton, J. R., Miller, P. A., Peng, C., Raivonen, M., Riley, W. J., Sonnentag, O., Aalto, T., Vargas, R., Zhang, W., Zhu, Q., Zhu, Q., Zhuang, Q., Windham-Myers, L., Jackson, R. B., and Poulter, B.: Characterizing Performance of Freshwater Wetland Methane Models Across Time Scales at FLUXNET-CH4 Sites Using Wavelet Analyses, J. Geophys. Res.-Biogeo., 128, e2022JG007259, https://doi.org/10.1029/2022JG007259, 2023b.

Zhu, Q., Peng, C., Ciais, P., Jiang, H., Liu, J., Bousquet, P., Li, S., Chang, J., Fang, X., Zhou, X., Chen, H., Liu, S., Lin, G., Gong, P., Wang, M., Wang, H., Xiang, W., and Chen, J.: Interannual variation in methane emissions from tropical wetlands triggered by repeated El Niño Southern Oscillation, Glob. Change Biol., 23, 4706–4716, https://doi.org/10.1111/gcb.13726, 2017.

Zona, D., Gioli, B., Commane, R., Lindaas, J., Wofsy, S. C., Miller, C. E., Dinardo, S. J., Dengel, S., Sweeney, C., Karion, A., Chang, R. Y.-W., Henderson, J. M., Murphy, P. C., Goodrich, J. P., Moreaux, V., Liljedahl, A., Watts, J. D., Kimball, J. S., Lipson, D. A., and Oechel, W. C.: Cold season emissions dominate the Arctic tundra methane budget, P. Natl. Acad. Sci. USA, 113, 40–45, https://doi.org/10.1073/pnas.1516017113, 2016.